Self-Assembled Monolayer on Silicon

Hiroyuki Sugimura

Department of Materials Science and Engineering,
Kyoto University
Sakyo, Kyoto 606-8501
hiroyuki-sugimura@mtl.kyoto-u.ac.jp

1. Introduction

Self-assembling, in which minute elements such as atoms, molecules and clusters are spontaneously organized into an ordered array of the elements, is a key process of the bottom-up nanotechnology [1-4]. One of the promising material processes on the basis of self-assembly is the fabrication of organic thin films with a monomolecular thickness. Although, it has been well-known that some types of organic molecules adsorb on a particular substrate and form a monolayer since several tens of years ago [5-7], such types of organic monolayers have recently named as self-assembled monolayers (SAMs). As schematically illustrated in Fig. 1, when a particular substrate is immersed in a solution of precursor molecules which have a chemical reactivity to the substrate surface, the molecules chemisorb on the surface with their reactive sites being faced to the surface. Most of the SAM precursors have a long alkyl chain or an aromatic ring so that some types of intermolecular interactions, e.g., van der Waals, hydrophobic and π-electron interactions, work between the chemisorbed molecules. Consequently, the molecules are attracted each other so as to be closely packed and to form a thin and uniform film with a monomolecular thickness. Due to immobilization of the molecules to the substrate through chemical bondings and the presence of intermolecular attractive interactions, SAMs are more stable mechanically, chemically and thermodynamically compared with similar monolayers fabricated by the Langmuir-Blodgett technique.

Once a SAM is formed on a substrate, its surface is entirely covered with organic molecules. Since there is no room on the surface to be further adsorbed with molecules, the SAM growth stops automatically at this stage. The thickness of the SAM is determined with the length of the precursor molecules and an adsorption angle of the molecules. There is no need for the precise control of process conditions in order to fabricate molecular-level ultrathin films with their thicknesses in the range of 1 ~ 2 nm. Besides thickness, the presence of a SAM on a substrate alters surface physical and chemical properties being markedly different from those of the bare substrate.

However, the formation of SAMs depends on unique chemical reactions between a substrate and organic molecules. Hence, specific pairs of a substrate and a precursor are required to fabricate SAMs. Typical examples for these SAM formation pairs are summarized in Table 1. Among various materials, Si is most important in micro ~ nano electronics and mechatronics. Thus, SAMs on Si are of special interest in order to integrate Si micro ~ nanodevices with organic molecules. As described in Section 2, there have been two major methods preparing SAMs on Si.

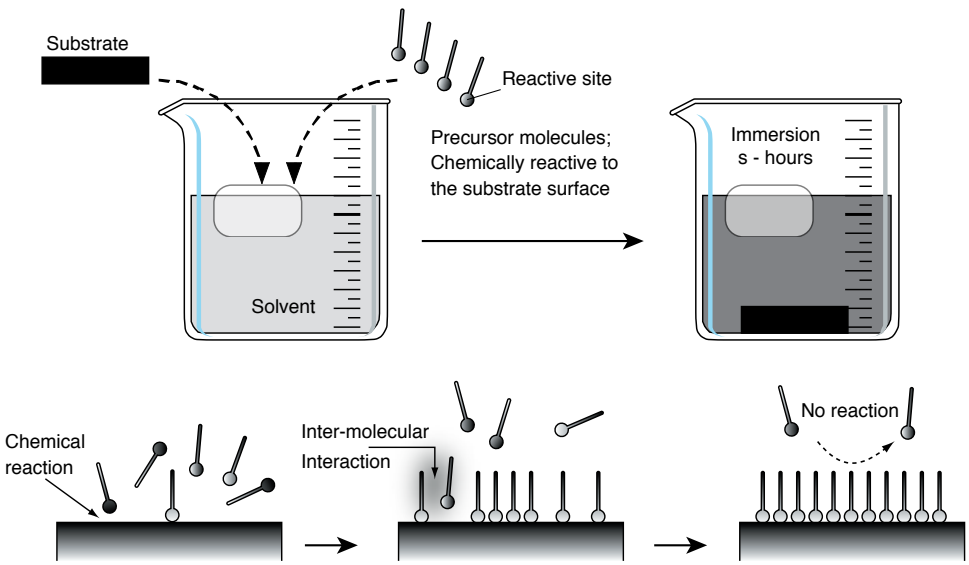

Figure 1. Preparation procedure for self-assembled monolayer (SAM).

Table 1 Pairs of precursors and substrates.

Precursor Molecules	Substrate Materials
Organosulfurs alkylthiol; R-SH dialkyldisulfide; RS-SR' thioisocyanide; R-SCN etc.	Metals/Compound Semiconductors Au, Ag, Cu, Pt, Pd, Hg, Fe, GaAs, InP
Fatty acid R-COOH	Oxide Al_2O_3, AgO, CuO
Phosphonic acid $R\text{-}PO_3H_2$	Oxide ZrO_2, TiO_2, Al_2O_3, Ta_2O_5, etc.
Organosilanes; $R\text{-}SiX_3$ (X = Cl, OCH_3, OC_2H_5)	Oxide glass, mica, SiO_2, SnO_2, GeO_2, ZrO_2, TiO_2, Al_2O_3, ITO, PZT, etc.
Unsaturated hydrocarbons alkene, alkyne; $R\text{-}CH{=}CH_2$, R-C≡H Alchols, Aldehydes R-OH, R-CHO	Silicon hydrogen-terminated Si; Si-H halogen-terminated Si; Si-X (X=Cl, Br, I)

2. Self-Assembled Monolayers on Si

2.1. SAM Formation on Oxide-Covered Si through the Silane Coupling Chemistry

A molecule consisting of one Si atom connected with four functional groups, SiX_4, is named as "silane". A molecule in which at least one of these four functional groups are substituted with organic functional groups, that is, SiR_nX_{4-n}, is organosilane. Organosilane molecules react with hydroxyl groups on an oxide surface so as to be fixed on the surface as illustrated in Fig. 2. This surface modification chemistry has been practically used as the silane coupling reaction for preparing organic layers on inorganic materials surfaces [8]. Sagiv and co-workers have reported, for the first time, that SAMs could be formed from organosilane molecules with one long alkyl chain in each of the molecules [9,10]. On a Si substrate, such a SAM can be formed as well by covering the substrate with its oxide.

As shown in Fig. 2, a trace amount of water is necessary to form organosilane SAMs. Halogen or alcohoxy groups in an organosilane molecule are converted to hydroxyl (-OH) groups by hydrolysis. Dehydration reaction

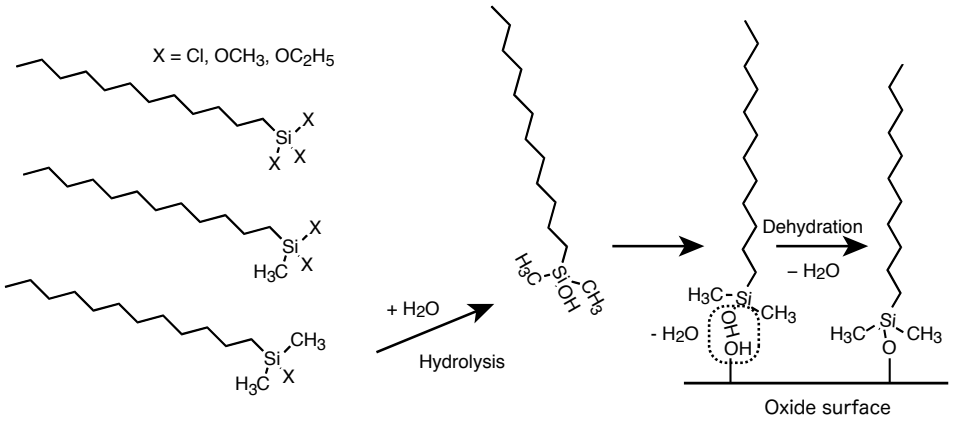

Figure 2. Organosilane SAMs.

between these silanol (Si-OH) sites in the molecule with -OH groups on the surface oxide of a Si substrate immobilizes the molecules on the oxide through siloxane (Si-O-Si) bonds.

There are three types of organosilane precursor molecules which have one, two or three reactive sites. When a SAM is formed from organosilane molecules with a single reactive site, the molecular density assembled into the SAM remains to be relatively low due to steric hindrance between methyl ($-CH_3$) groups of adjacent molecules. On the other hand, when a SAM is formed from organosilane molecules each of which has three reactive sites, its growth behavior is complicated somewhat. Since two Si-OH groups remain in the organosilane molecule after that is immobilized on the substrate, the molecule is further linked with adjacent organosilane molecules through Si-O-Si bonds as illustrated in Fig. 3. This type of organosilane SAM is more closely packed and stable mechanically, chemically and thermally due to the siloxane network laterally connecting molecules in the SAM in addition to the chemical attachment to the substrate.

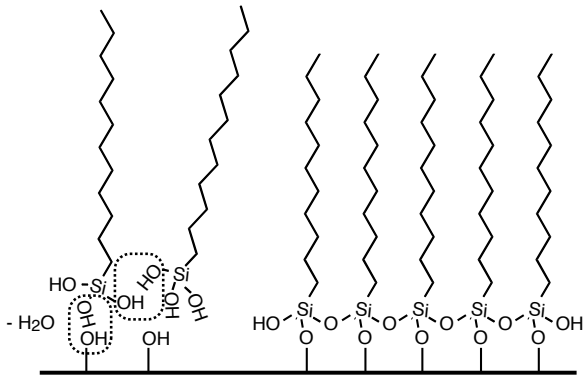

Figure 3. SAM formation from tri-functional organosilane molecules.

2.2. SAMs directly bonded to Si

If a SAM can be formed on a semiconductor surface, it is expected to be a springboard for integrating functionalities of semiconductors and organic molecules. Although, the silane-coupling method described in Section 2.1. is powerful and indispensable for the preparation of SAMs on Si, the organosilane SAMs have a disadvantage from the viewpoint of electronic applications. Such SAMs require the presence of a thin oxide layer, namely, a very good insulator, of 1 ~ 2 nm in thickness at least on Si substrates. Therefore, in this case, we can utilize electronic functions of the SAMs only in the situation inserting the insulator between SAM and Si. An alternative technology is needed in order to form SAMs on Si without its surface oxide.

Such a process technique has been reported in 1993 by Linford and Chidsey [11] and, thereafter, extended markedly by them and other researchers [12]. In general, Si radicals are first formed by extracting hydrogen atoms from a hydrogen-terminated Si surface or halogen atoms from a halogen-terminated Si surface, usually by the use of a reaction initiator, thermal excitation or photo irradiation. Some types of organic molecules are covalently immobilized on Si through a reaction with the Si radicals. As shown in Fig. 4, for example, an 1-alkene molecule reacts with a mono-hydrated Si(111) surface and is connected to the surface through a Si-C bond. The remained C radical extracts a H atom from an adjacent Si-H resulting in the formation of a Si radical again. The chain reaction proceeds by repeating these reactions. Steric hindrance between the organic molecules limits the replacement degree of H with R to be about 50% at most [13].

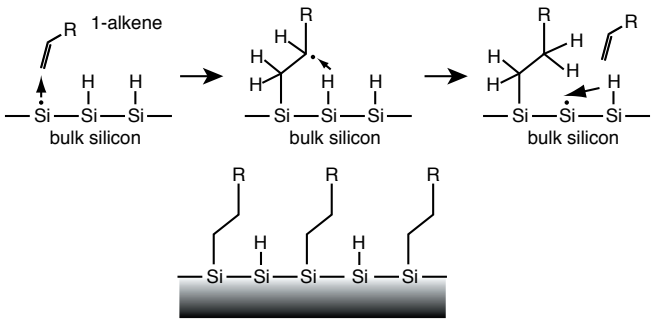

Figure 4. SAM formation on Si through the radical reaction.

3. Vapor phase growth of organosilane SAM

3.1. SAM formation at the vapor/solid interface

Organosilane SAMs are formed on OH-bearing oxide surfaces through the chemical reaction of organosilane molecules with the OH sites. The SAMs were usually prepared at the liquid/solid interface by simply immersing a substrate in a solution of precursor molecules [10,14]. Besides this liquid phase process, the vapor phase process [15-24] is also promising particularly because it has no need for the use of a large amount of solvents which are necessary in the liquid phase processes. Furthermore, particulate deposits of aggregated organosilane molecules, which frequently degrades the quality of the SAMs, is expected to be fewer in the vapor phase method than in the liquid phase method, since such aggregated molecules have lower vapor pressures and are rarely vaporized. Thus, the vapor phase method is considered to be practically convenient, although the method is not widely applicable at present since it depends whether a precursor can vaporize or not, and the molecular ordering of vapor-grown SAMs is inferior to that of liquid-grown SAMs [23].

3.2. Preparation procedure

Organosilane SAMs were formed through a simple method described as follows [21]. Here, we demonstrate results on three types of precursors, that is, n-octadecyltrimethoxysilane [ODS: $H_3C(CH_2)_{17}Si(OCH_3)_3$], n-(6-aminohexyl)aminopropyltrimethoxysilane [AHAPS: $H_2N(CH_2)_6NH(CH_2)_3Si(OCH_3)_3$], and fluoroalkylsilane (FAS), heptadecafluoro-1,1,2,2-tetrahydro-decyl-1-trimethoxysilane [$F_3C(CF_2)_7(CH_2)_2Si(OCH_3)_3$]. The chemical structures of these precursors and their corresponding SAMs are shown in Fig. 11. A photocleaned SiO_2/Si plate was placed together with a glass cup filled with organosilane liquid into a Teflon™ container. When ODS and FAS were employed, the container was sealed with a cap and placed in an oven maintained at 150 ˚C. In the case of AHAPS, organosilane liquid diluted with toluene under dry N_2 atmosphere in order to avoid gelation of AHAPS through polymerization. A lower temperature of 100 ˚C was employed for AHAPS in order to minimize polymerization of AHAPS in toluene. Subsequently each of the samples treated with AHAPS were sonicated for 20 min with successive in dehydrate ethanol and dehydrate toluene. Then, the samples were further sonicated in NaOH (1 mM) and HNO_3 (1 mM) in order to remove excessively adsorbed AHAPS molecules. Finally, the samples were rinsed with Milli-Q water and were blown dry with a N_2 gas stream.

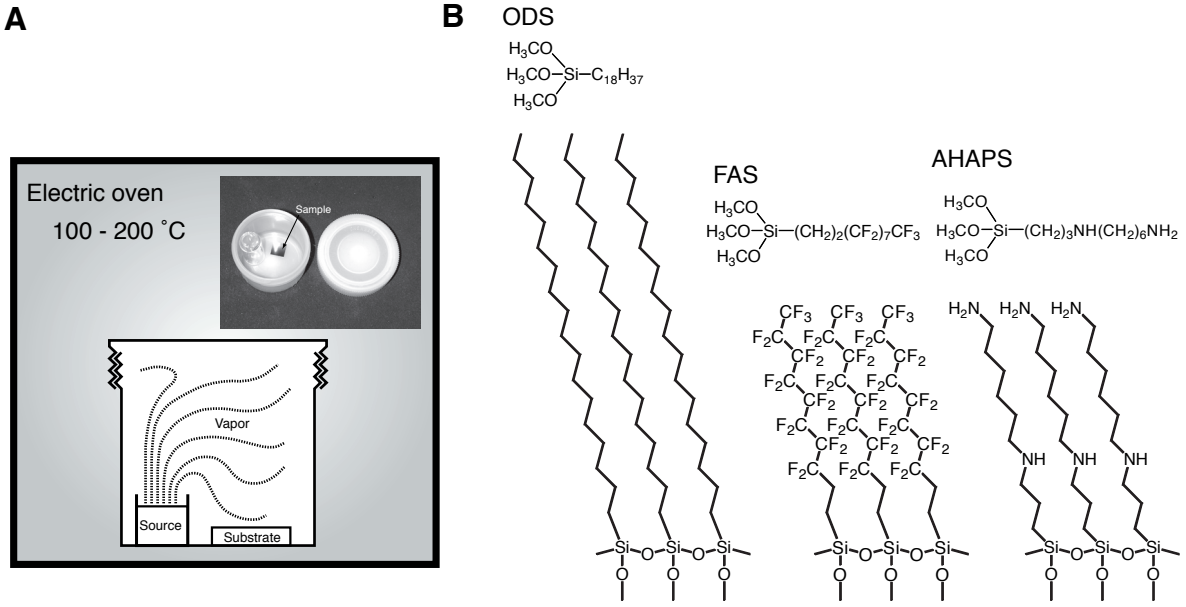

Figure 5. A) Organosilane vapor treatment in a closed vessel, B) Chemical structures of precursor molecules and corresponding SAMs.

3.3. Vapor-grown organosilane SAMs

Organosilane molecules in a vapor or liquid phase react with OH groups on an oxide surface resulting in the formation of a SAM as illustrated in Fig. 3. Figures 5A and 5B follow the formation of ODS-, FAS- and AHAPS-SAMs. When a SiO_2/Si substrate is treated with ODS or FAS, it becomes hydrophobic as shown in Fig. 2. The water contact angles of the ODS and FAS-treated substrates increased with an increase in reaction time at the initial stage. However, they hardly increased even when the process had been prolonged longer than 3 and 1 hours, in the cases of ODS and

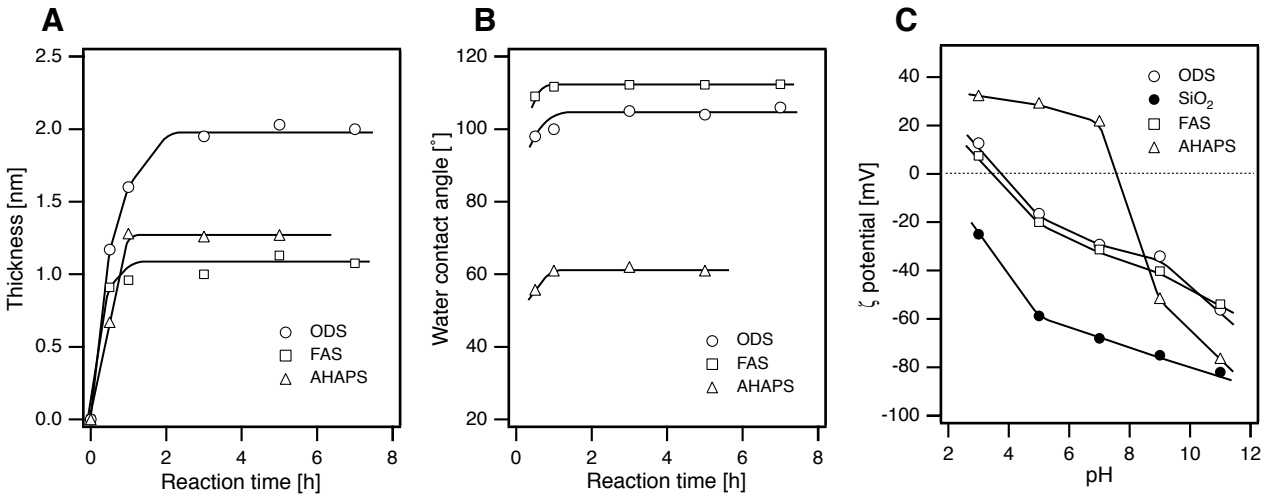

Figure 6. Organosilane SAMs grown by the vapor phase method. A) Thickness, B) Water contact angle and C) ζ potential.

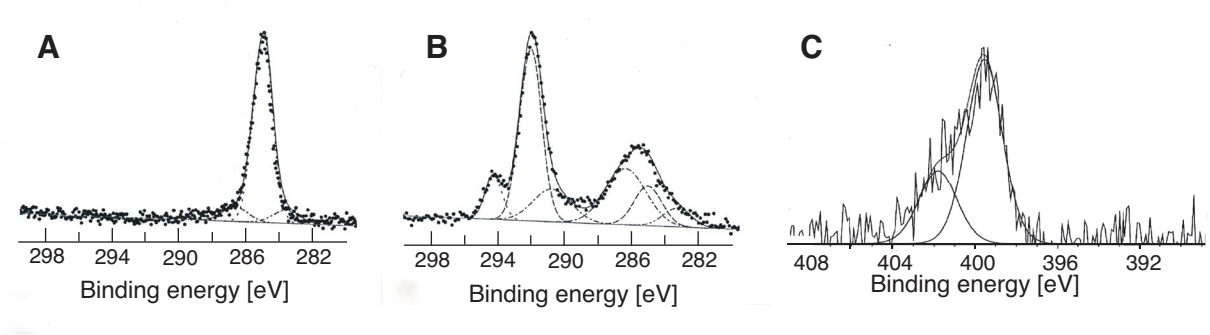

Figure 7. XPS spectra of the organosilane SAMs. A) C1s spectrum of ODS-SAM, B) C1s spectrum of FAS-SAM and C) N1s spectram of AHAPS-SAM.

FAS-treated substrates, respectively. The water contact angles of the ODS and FAS-treated substrates reached 105° and 112°, respectively. XPS-C1s spectra of the deposited films are shown in Fig. 7. The spectrum of the film prepared from ODS (Fig. 7A) consists almost of a single peak centered at 285.0 eV, indicating that a hydrocarbon film corresponding to its precursor was formed. On the other hand, the spectrum of the film prepared from FAS (Fig. 7B) could be resolved into 6 features, centered at binding energies of 283.5-283.6, 285.0, 286.6-286.7, 290.5, 291.7-291.9 and 294.1 eV. These components correspond to Si-C, C-C, C-O, -$\underline{C}F_2$-CH_2-, -CF_2-CF_2- and $\underline{C}F_3$-CF_2- groups, respectively. The film deposited form FAS is a fluorocarbon film which is more hydrophobic than the hydrocarbon film.

As clearly demonstrated in Fig. 6B, that is a graph of the films' thicknesses as estimated by ellipsometry, the thicknesses of the ODS and FAS films increase and stop to increase similarly. A film of 2 nm thick was grown on the ODS-treated substrate at a reaction time of longer than 3 hours, while a film of 1.1 nm thick was formed on the substrate treated with FAS for longer than 1 hour. These thicknesses of the deposited films are shorter than the lengths of the corresponding precursor molecules; Those are 2.35 and 1.34 nm for ODS and FAS, respectively. The both deposited films are thus considered to be monomolecular layers composed of packed molecules inclined more than 30° to normal. ODS has a vapor pressure of 2 Torr at 150 °C, while FAS's vapor pressure is 1 Torr at 86 °C. Thus, FAS is expected to show a higher vapor pressure than ODS at our preparation temperature of 150 °C. This is the reason why ODS took a longer time to form a monolayer than FAS did.

Besides ODS and FAS, AHAPS forms a monolayer as well. Its thicknesses reach 1.3 nm at a reaction time of 1 hour and remained unchanged even when the reaction time was extended up to 5 h. However, unlike the other SAMs prepared from ODS and FAS, the AHAPS-SAM formation was not reproducible when it was conducted without the sonication in the organic solvents and in the ionic solutions. Since an amino group in the aminosilane molecule, that is, -NH_2 or –NH-, may form a hydrogen or ionic bond with a methoxysilane group or its hydrolysis form, that is, $SiOCH_3$ or SiOH, respectively, in another aminosilane molecule, AHAPS molecules are thought to form aggregates and to be further adsorbed on the AHAPS-SAM surface. Indeed, thicknesses of the AHAPS deposits prior to the sonication were sometimes 2~3 times greater than the true thickness of the AHAPS-SAM. A considerable amount of AHAPS molecules were thought to be adsorbed on the SAM surface. The thickness of the AHAPS-SAM, that is, 1.3 nm, is slightly smaller

than the calculated molecular length of 1.48 nm. The adsorbed AHAPS molecules formed a monolayer but probably inclined about 25° to normal. Although simply physisorbed AHAPS molecules can be removed by the sonication in the organic solvents, the chemisorbed AHAPS molecules through hydrogen and ionic bondings still remain. This is the reason why the sonication in the ionic solutions was needed.

Water-contact angles of the AHAPS-treated substrates also increased with the reaction time, as indicated by open triangles in Fig. 6A. The atomic ratio of nitrogen to carbon (N/C) of the AHAPS-SAM was estimated to be about 0.17 from its XPS. This is slightly smaller than that of the chemical formula of AHAPS molecule (N/C = 0.19) probably due to adventitious carbon contaminants on its surface. As shown in Fig. 8, an N1s XPS peak consists of at least two chemical components with binding energies at 399.6 and 400.9 eV. The former is assigned to –NH- and -NH_2 groups while the later corresponds to the protonated amino groups. The AHAPS-SAM is found to be protonated partially, probably due to washing in the acidic solution in the preparation process.

Figure 6C depicts the variation in ζ-potentials of the ODS-SAM (open circle), FAS-SAM (open square), AHAPS-SAM (open triangle) covered, and uncovered SiO_2/Si substrates (closed circle). These ζ-potentials were measured at a temperature of 298 K by the use of an electrophoretic light scattering spectrophotometer as described in detail elsewhere [25]. A solution containing 1 mM-KCl as supporting electrolyte was used, adjusting its pH over the range of 3–11 by adding HCl or NaOH. Each ζ-potential was estimated from the average of the values measured three times. The error of the ζ-potentials was about ±5 mV. In the pH range of 3 to 11, the SiO_2/Si substrate shows negative ζ-potentials of ca. 25 to 82 mV due to partial ionization of the surface silanol groups (SiOH) to –SiO^-, similar to silica particles [26.27]. Although there are no isoelectric point (IEP) in this pH range, by extrapolating the potential curve, the IEP of the SiO_2/Si substrate is estimated to be pH 2.0 coinciding with the reported IEP of silica [28].

The pH dependence of the ζ-potentials for the ODS and FAS-SAM on the SiO_2/Si substrates is significantly different from those of the naked SiO_2/Si substrate. These ζ-potential vs. pH curves are nearly identical in shape and magnitude in the entire pH range. From the potential curves, the negative ζ-potentials of the ODS and FAS-SAM covered samples are approximately 35 ~ 65 % lower in magnitude than those of the naked SiO_2/Si substrate. This is attributable to the reduction of the number of silanol groups on the SiO_2/Si surface since they are consumed through the covalently bonding at the SAM-SiO_2/Si interface. Furthermore, the IEPs of the ODS and FAS-SAM covered samples are estimated to be pH 3.5 ~ 4.0. This IEP value is higher than the IEP of the naked SiO_2/Si substrate, that is, pH 2.0, and are almost same with IEPs of polyethylene and polytetrafluoroethylene plates, whose surfaces are terminated with -CH_2- and -CF_2- groups, respectively [27]. On the other hand, the AHAPS-SAM covered sample shows an IEP of pH 7.5 ~ 8.0. Its ζ-potentials are positive below pH 7.0. Under such acidic conditions, amino groups on the AHAPS-SAM are considered to be protonated to –NH_3^+. On the contrary, under basic conditions, the amino groups are probably converted to –NH^- or –NH_3O^- due to deprotonatiton or attachment of hydroxyl anions, resulting in large negative ζ-potentials as shown in Fig. 6C.

4. SAMs covalently bonded on Si

4.1. Chemical reactions of hydrogen-terminated Si surface

As described in Section 2.2., SAMs covalently bonded to bulk Si can be formed on the basis of chemical reactions of hydrogen-terminated Si (Si-H) surfaces with some types of organic molecules. Thermal activation, by which Si-H bonds on a substrate surface are thermally excited and dissociated typically at a temperature higher than 100 °C, are most commonly employed [29]. Si radicals, that is, dangling bonds, are consequently formed on the surface so as to act as reaction sites with organic molecules. In addition to molecules containing a carbon-carbon double or triple bond such as alkenes and alkynes [29,30], primary alcohol and aldehyde molecules are reported to react as well resulting in the formation of SAMs with Si-O-R forms [31].

Besides the thermal method, photoactivation of Si-H by irradiating with ultraviolet (UV) light less than 400 nm in wavelength has been successfully applied to form SAMs from alkenes, aldehydes and so forth [32-34]. This photochemical process has some advantages over the thermal process. One is that the photoprocess can be conducted at room temperature. Thus, the method applicable to SAM formation of thermally unstable molecules. Another is the capability in micropatterning. SAMs were successfully grown only in a selected area on a Si surface where had been irradiated with UV light through a photomask [32]. Recently, a photoactivation process using visible light at 488 nm has been employed in order to form SAMs on Si [35]. In this case, electron-hole pairs generated by excitation of the substrate Si are considered to promote chemical reactions, since photon energy of the visible light is too low to dissociate Si-H. The visible light process is certainly useful in the case of a precursor unstable with UV irradiation.

4.2. Hexadecyl and hexadecyloxy monolayers on Si

In this section, actual examples of SAMs covalently-bonded to bulk Si are described. Cleaned Si(111) substrates (phosphorus-doped n-type wafers with a resisitivity of 10-50 Ωcm) were first etched in 5% HF for 5 min at room temperature. Next, the substrates were treated in 40% NH_4F for 30 s at a temperature of 80 °C. Through these treatments, a surface oxide on each of the Si substrates was removed and the substrate surfaces became terminated with hydrogen. Due to this hydrogen termination, the substrate surfaces became hydrophobic somewhat so that their water contact angles increased to 80 - 85° from those of before oxide etching. The surface was initially covered with hydroxyl-

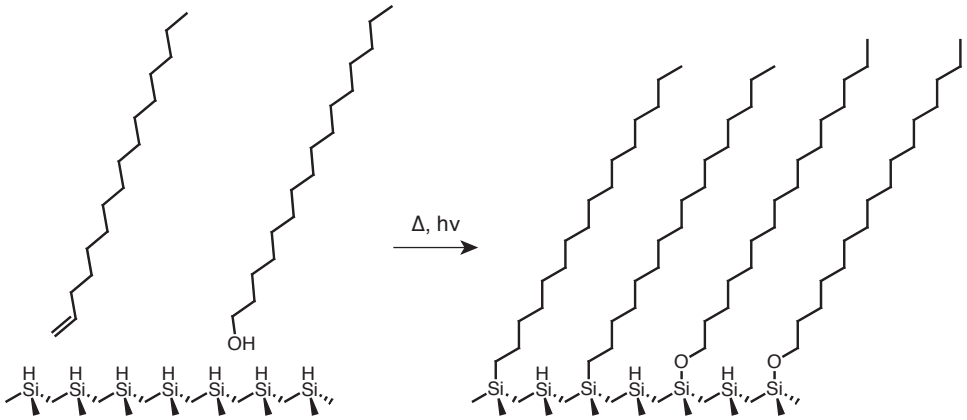

Figure 8. SAM formation on SiH from 1-hexadecene and 1-hexadecanol.

ated oxide showing a water contact angle almost 0°. Some of the Si-H substrates were treated in 1-hexadecene ($C_{16}H_{32}$) liquid, and the other ones were processed in a solution of 1-hexadecanol ($C_{16}H_{33}OH$) in mesitylene at a concentration of 10 mM. Before and throughout the reaction, a stream of nitrogen was bubbled into the liquid or the solution in order to purge oxygen from the entire reaction system and to suppress the Si-H surfaces being oxidized. For UV excitation, a super high-pressure Hg lamp was used without filtering. Thus, in addition to its main radiation peaks at 365, 405 and 436 nm, the radiated light contains some amounts of visible light. However, as reported in Ref. 32, UV components less than 380 nm in wavelength plays a central role in the activation of Si-H. A white light from a Xe lamp in the wavelength range from 400 to 800 nm was used for experiments activated with visible light.

As schematically illustrated in Fig. 8, the 1-alkene or primary alcohol molecules react with a Si-H surface to form corresponding hexadecyl (HD-SAM, Si-$C_{16}H_{33}$) or hexadecyloxy (HDO-SAM, Si-O-$C_{16}H_{33}$) monolayer, respectively. Table 2 summarizes water contact angles of HD- and HDO-SAM surfaces prepared by the thermal, UV and visible activation processes. The substrate surfaces become further hydrophobic to show water contact angles more than 105° , since those have been terminated with methyl (-CH_3) groups owing to the alkyl or alkoxy monolayer grown on each of the substrates. Figure 9 shows topographic images of the thermally-grown HD- and HDO-SAM surfaces acquired by AFM in the contact mode. Even after forming SAMs of about 2 nm thick, structures of Si(111) surface consisting of flat terraces separated with a monoatomic step of near 0.3 nm high are clearly retained.

Table 2 Water contact angles of HD- and HDO-SAMs.

SAM	Activation	Temperature	Reaction time	Water contact angle
HD	Thermal	180 °C	2 hours	109°
	UV / 660 mWcm^{-2}	R.T.	10 hours	107°
	Vis / 15 mWcm^{-2}	R.T.	15 hours	106°
HDO	Thermal	150 °C	2 hours	108°

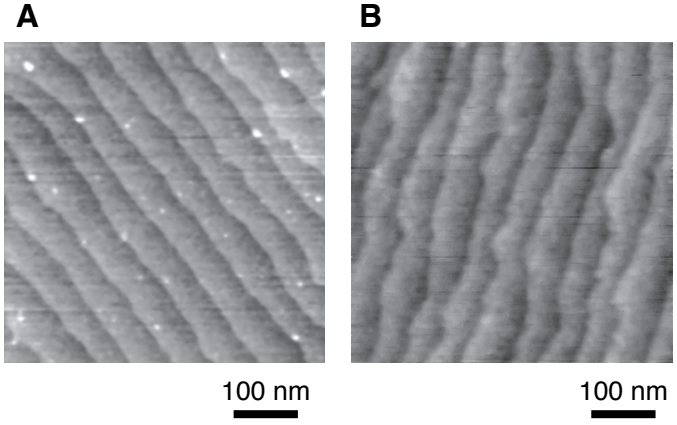

Figure 9. Topographic images acquired by AFM. A) HD-SAM covered Si(111) surface. B) HDO-SAM covered Si(111) surface.

As shown in Fig. 10A, an XPS-C1s spectrum for the HD-SAM on Si prepared by the thermal activation, the carbon signal corresponds to alkyl chains has been detected. The thickness of HD-SAM was in the range of 2.0 ~ 2.4 nm as estimated by ellipsometry. Figure 10A shows XPS-Si2p spectra of HD-SAM/Si, Si-H and Si covered with an oxide layer of about 2 nm thick. There are two peaks corresponding to Si^{4+} (oxidized Si) and Si^{0} centered near 103 and 99 eV, respectively, in the spectrum of the oxide-covered Si indicated by a broken curve. Such an oxidized Si peak is not present in the spectrum of the Si-H sample as indicated by a dotted curve. As confirmed by the spectrum of the HD-SAM sample indicated as a solid curve in Fig. 10B, there is no oxidized Si on this sample as well. This is an evidence that the monolayer is attached to bulk Si without an interfacial oxide layer, on the contrary to organosilane SAMs.

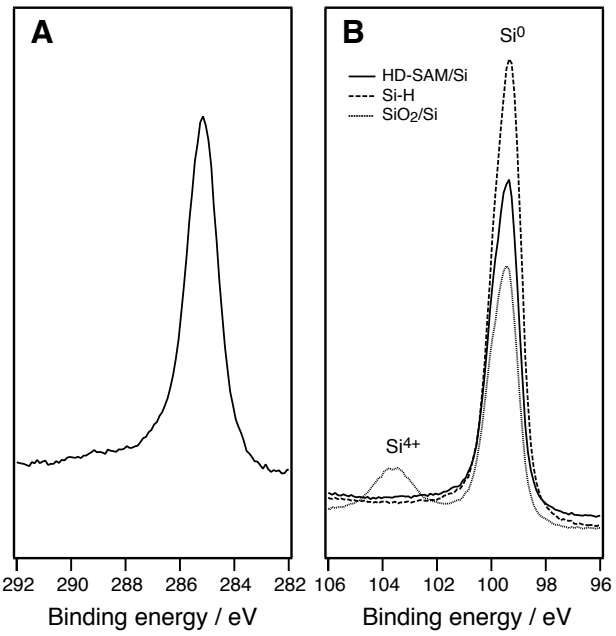

Figure 10. A) XPS-C1s spectrum of a HD-SAM/Si surface. B) XPS-Si2p spectra of HD-SAM/Si, Si-H and SiO2/Si surfaces.

As reported in Ref. 13, almost 50% of Si-H groups are considered to remain at the monolayer/Si interface. If these Si-H groups are exposed to air, those gradually dissociate and the underlying Si surface oxidizes, since Si-H is in a metastable state. Nevertheless, the XPS-Si2p spectrum of the HD-SAM sample shows the absence of Si oxide. This result indicates that the monolayer formed on Si is tightly packed and the remained Si-H groups are effectively shielded. It was confirmed as well that there were no Si oxide on the other SAM samples photochemically prepared from 1-hexadecene and thermally prepared from 1-hexadecanol shown in Table 2.

5. SAMs on Si in micro - nano patterning

5.1. SAMs as ultra thin resist films for patterning

For advanced applications of SAMs in microdevices with mechanical, electronic, chemical and biological functions, micro - nano structuring technologies for the SAMs are of primary importance [36-41]. Among various patterning methods, photolithography has been commonly employed, since the technique is most practical mainly due to its high throughput.

Besides photolithography, other lithographic methods including electron beam irradiation [42-47], ion beam etching [48], neutral atomic beam exposure [49-51], X-ray lithography [52-56] have been used in order to fabricate micro ~ nanopatterns on various types of SAMs. Furthermore, a unique method, so-called μ-contact printing, in which micropatterns are printed on a solid substrate using a microstructured silicone rubber as a stamp and a solution of precursor molecules as an ink, has been developed and improved rapidly in recent ten years [37,38,57-60]. Another promising nanopatterning method is a nanolithography based on scanning probe microscopy as described in Section 5.5.

5.2. Photopatterning of organosilane SAMs

Photopatterning of SAMs on Si was reported for the first time by the research group in Naval Research Laboratory, USA [36, 61-64]. They employed excimer lasers of 248 and 192 nm in wavelengths in order to induce particular photochemical reactions of organosilane SAMs, for example, dissociation of Si-C bonds trough excitation of the adjacent aromatic rings [61] as illustrated in Fig. 11A. The method has been extended to deactivation of -NH_2 groups

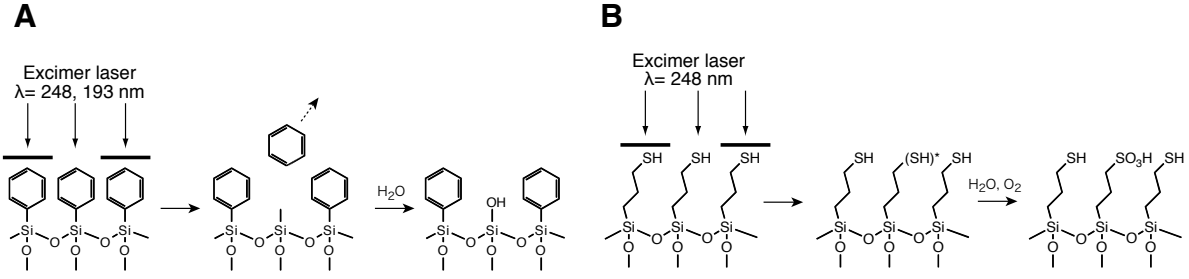

Figure 11. Examples of UV exposure. A) Dissociation of phenylsilane SAM through the exciation of aromatic rings. B) Photochemical converstion of SH to SO_3H.

and oxidation of -CH_2Cl groups. We have also reported that photochemical conversion of surface SH and -SS- groups to SO_3H groups using an excimer laser at 248 nm as illustrated in Fig. 11B [65].

These approaches are successful for fabrication of micropatterns on organosilane SAMs, the photochemical reactions governing the processes depend on the particular functional groups, such as phenyl, amino and mercapto groups, so that the methods are not applicable generally to other organosilane monolayers, including alkylsilane and fluoroalkylsilane SAMs, in spite of the fact that theses SAMs are frequently used for surface modification. We have developed a promising way applicable to any types of organic thin films [66-72].

The method is based on the use of vacuum ultra-violet (VUV) light at a wavelength of 172 nm radiation from an excimer lamp. Why a VUV light of 172 nm in wavelength is used? One crucial advantage is its high photon energy of 7.2 eV. Such high energy photons can excite a variety of organic molecules which has no photosensitivity to UV lights with a longer wavelength usually used in photolithography. Furthermore, the VUV light of 172 nm in wavelength dissociates oxygen molecules into two oxygen atoms in the singlet and triplet states, [O(1D) and O(3P), respectively] as described in Eq. 1 [73].

$$O_2 + h\nu \rightarrow O(1D) + O(3P) \qquad (1)$$

Since these oxygen atoms, particularly O(1D), have oxidative reactivities strong enough to oxidize alkyl and fluoroalkyl chains which are hardly decomposed by the irradiation with VUV light at 172 nm alone. VUV-micropatterning rates of SAMs are distinctly accelerated through the simultaneous VUV excitation of the SAMs and oxygen molecules existing on and around the SAM surfaces.

Several types of excimer lamps which radiating VUV light with a shorter wavelength than 172 nm have been developed as well. Such short-wavelength VUV lights are more favorable for promoting surface modification reactions of organic monolayers, since those can induce direct excitations of C-C and C-H bonds. Nevertheless, VUV light of 172 nm is advantageous in respect of practical applications. At 172 nm, quartz has an adequate transparency so as to be applicable as a material for optical parts. Quartz-made optical parts including photomasks are frequently used in common photolithographic processes and are readily available. This is the second advantage of VUV lithography at 172 nm.

As schematically illustrated in Fig. 12A, a sample (a SiO_2/Si substrate covered with ODS-SAM prepared by the vapor phase method as described in Section 3) was micropatterned by a mask-contact photolithography. A sample being

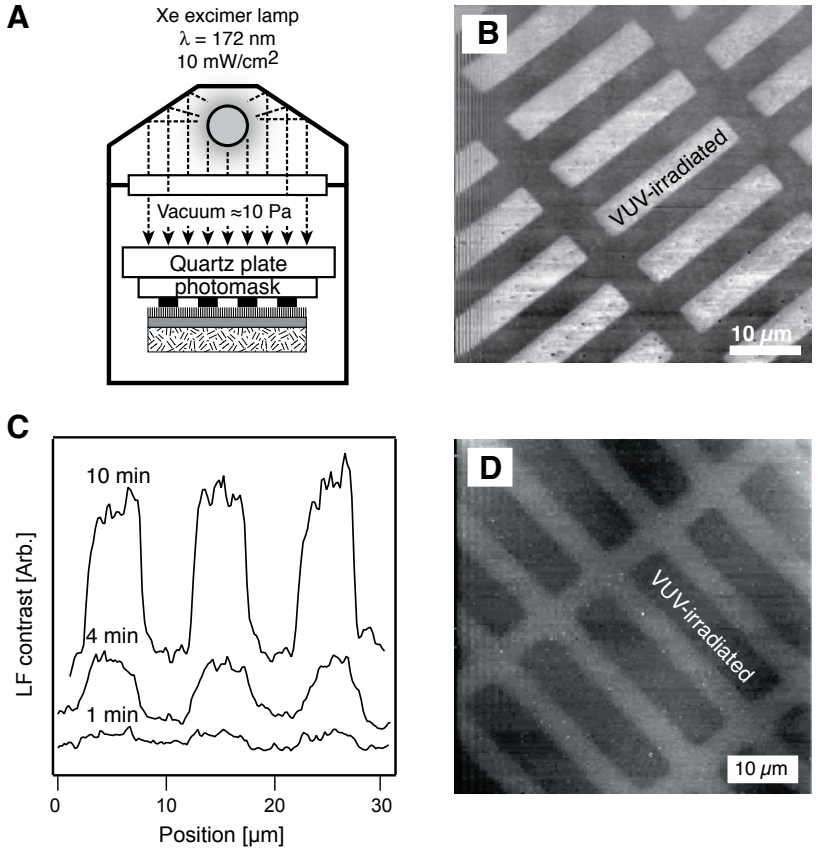

Figure 12. VUV lithography. A) VUV micropatterning apparatus. B)LFM image of ODS-SAM irradiated for 10 min through the photomask. C) Cross sections of LF images for the samples irradiated for 1, 4 and 10 min. D) Topographic AFM image of the ODS-SAM irradiated for 20 min.

placed with a photomask was located in a vacuum chamber of which pressure was controlled by introducing air through a variable leak valve. A weight, the quartz glass plate of 10 mm thick, was put on the photomask in order to attain a satisfactory contact between the mask and the SAM surface.

Figure 12B shows a lateral force microscope (LFM) image of the sample irradiated for 10 min with VUV light through the photomask. This VUV irradiation was performed at a pressure of 10 Pa. The image consists of two distinct regions which are bright 5 μm × 25 μm rectangular features and a dark surrounding area. These bright features correspond to the VUV-irradiated regions that possess a higher friction coefficient than that of the unirradiated ODS-SAM. Such an image contrast becomes more distinct with an increase in irradiation time. As shown in Fig. 12C, at an irradiation for 1 min, an LFM contrast is faint while, at irradiation periods of 4 and 10 min, the contrasts become ca. 6 and 40 times greater, respectively. The LFM contrast became to increase unrapidly when VUV irradiation was further prolonged and finally became to be almost unchanged at irradiation times more than 15 min, at which ODS-SAM was considered to be almost removed as expected from other experimental results such as water contact angle measurements, X-ray photoelectron spectroscopy (XPS) and infra-red reflection absorption spectroscopy. Indeed, as confirmed by an topographic AFM image shown in Fig. 12D, regions VUV-irradiated for 20 min are recessed about 1.5 ~ 2.0 nm. This depth corresponds to the thickness of ODS-SAM.

5.3. Photopatterning of the hexadecyloxy SAM

The VUV-patterning method described in Section 5.2. is applicable to SAMs covalently bonded to Si as well [75-77]. In this section, VUV-patterning of HDO-SAM is described. First, the VUV-degradation chemistry of HDO-SAM was studied based on XPS. Figures 13A, 13B and 13C show XPS-C1s, -O1s and -Si2p spectra, respectively, of the monolayer-covered Si samples prior to VUV-irradiation and VUV-irradiated for 120 and 480 s at a pressure of 10^3 Pa. By the VUV-irradiation at 10^3 Pa for 120 s, the amount of carbon on the sample decreases. On the contrary, the amount of oxygen on the sample increases. As indicated in the binding energy range between 287 ~ 289 eV of the XPS-C1s spectrum, polar functional groups containing oxygen have been formed. Accordingly, the sample surface became hydrophilic. Owing to the polar functional groups themselves and an increased amount of water molecules onto the hydrophilic surface, the O1s signal intensity increased.

As can be seen in Fig. 13C, the XPS-Si2p spectrum of the monolayer without VUV-irradiation has only a single peak near 100 eV, indicating that no oxide is formed between the Si substrate and the monolayer. At the irradiation time of 120 s, no oxide is still present at the monolayer-substrate interface. The Si2p signal from the substrate increases, since the monolayer thickness has decreased. Finally, at an irradiation time of 480 s where the monolayer has been considered to be completely decomposed, the C1s signal further decreases. This intensity is almost equal to a C1s signal caused by a contamination layer which always adsorbs on the sample surface before brought into the measurement chamber of XPS. Thus, the alkyl part of the monolayer has been recognized to be almost removed form the substrate. It is noteworthy that an additional peak centered around 103 eV is appeared in the XPS-Si2p spectrum. Furthermore, the O1s signal increases markedly. These results indicate that silicon oxide is formed on the sample surface. The oxide thickness was estimated to be about 1.5 nm by ellipsometry.

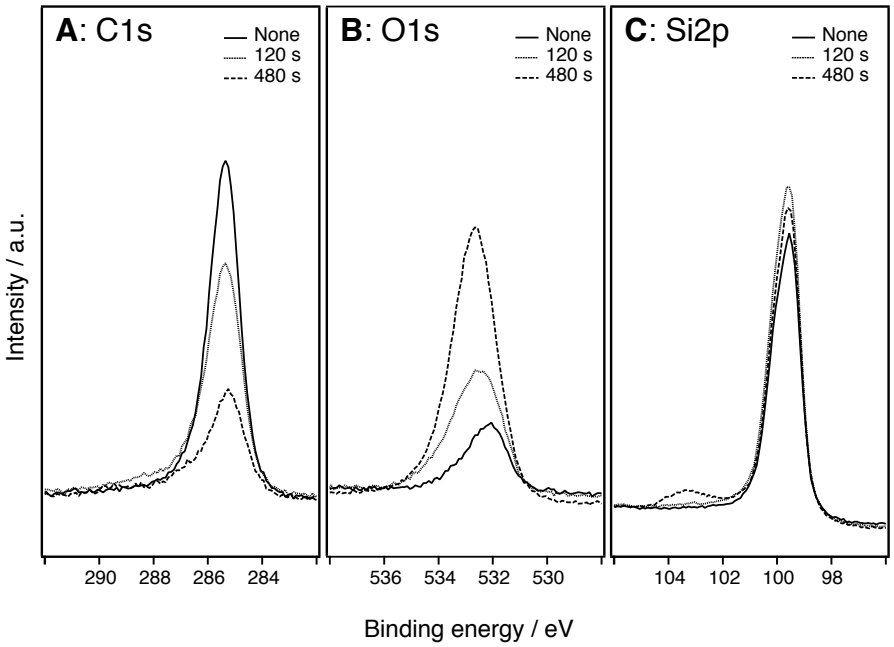

Figure 13. XPS-C1s, O1s and Si2p spectra of HDO-SAM surfaces unirradiated and irradiated with VUV light for 120 or 480 s.

Two of microfabrication processes based on VUV-photolithography and HDO-SAM are demonstrated here. As schematically illustrated in Fig. 14A, the monolayer was VUV-photoetched and a Si oxide layer grown in the VUV-irradiated regions. One of these VUV-patterned samples was treated with HF. The oxide layer grown on the VUV-irradiated region is etched, while the monolayer is resistant to HF. Thus, as illustrated in Fig. 4B, dimples are formed on the sample surface through the selective etching of the oxide. As shown in the AFM topographic image, the VUV-irradiated region is distinctly depressed from the surrounding area where is covered with the monolayer. The monolayer has successfully worked as an etching mask. Such a resistiviy to HF etching is a characteristic feature of organic monolayers covalently attached to Si substrates [78], on the contrary to organosilane monolayers fixed on Si with inserting an oxide layer. For example, ODS-SAM on oxide-covered Si could resist only for a few seconds or less even in 2% HF solution [79].

In the next demonstration, the VUV-patterned sample was treated with ODS by the vapor phase method described in Section 3, in order to form an organosilane monolayer on the oxide surface fabricated by the VUV-exposure. The details of this organosilane monolayer growth by the vapor phase method has been reported in Section 3. The oxide surface has an affinity to the silane coupling chemistry with organosilane molecules, while the monolayer-covered surface does not react with the organosilane molecules. Accordingly, an organosilane monolayer are formed selectively on the VUV-grown oxide surface, as illustrated in Fig. 14C. The AFM topographic image indicates that the VUV-exposed region protrudes from the region covered with HDO-SAM.

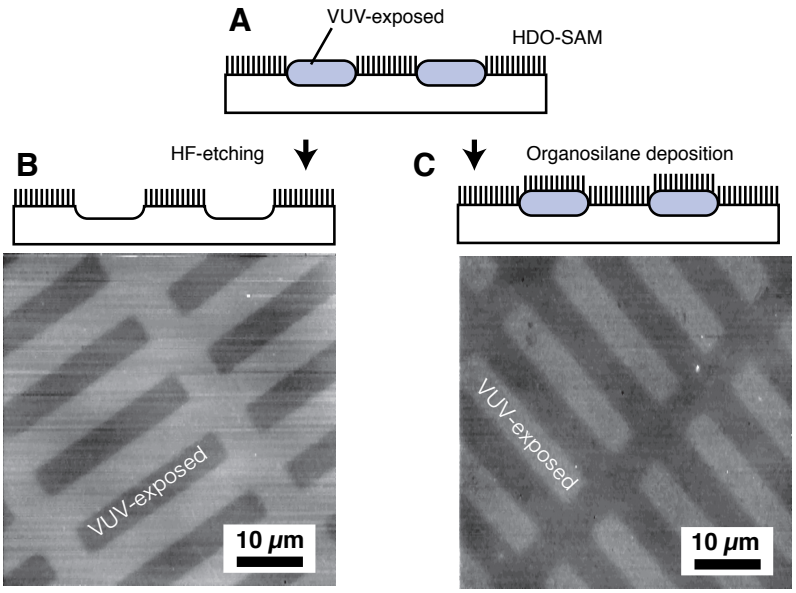

Figure 14. VUV-photolithography process. A) A micropatterned HDO-SAM/Si sample. VUV-patterning was conducted at an exposure time for 480 s and a camber pressure of 10^3 Pa. B) Etching in 5% HF solution for 5 min. C) organosilane deposition on the VUV-grown oxide surface.

5.4. VUV lithography system

The VUV-induced degradation rates of the SAMs are governed mainly by the two factors. The first is the intensity of VUV light at the SAM surface. The second is the amount of oxygen supplied to the surface. In the present case as depicted in Fig. 12A, it is difficult to satisfy these two factors simultaneously since the VUV light intensity decreases when the chamber pressure is increased in order to supply oxygen molecules much more. Hence, we have constructed a new VUV lithography system as schematically illustrated in Fig. 15 [80,81]. In this system, a sample is placed in air in order to supply a large amount of oxygen, while the space between the photomask and the lamp window is purged with nitrogen to avoid the absorption of VUV light with oxygen molecules. Namely, the photomask works as a separation wall between the nitrogen and air atmospheres. Furthermore, a proximity gap between the photomask and the sample is controlled precisely at an accuracy of 0.1 μm using a mechanical stage.

The performance of this VUV-exposure system was characterized by measuring water contact angles of VUV-irradiated ODS-SAM samples. The ODS-SAM surface becomes hydrophilic due to VUV irradiation, since polar functional groups have been formed through oxidation of the alkyl chains. Finally, at a certain VUV-dose, its surface completely wetted with water showing a water contact angle of almost 0°, when all the ODS molecules had been decomposed and removed so that the underlying SiO_2 surface had been appeared. As shown in Fig. 16A, a VUV-dose of

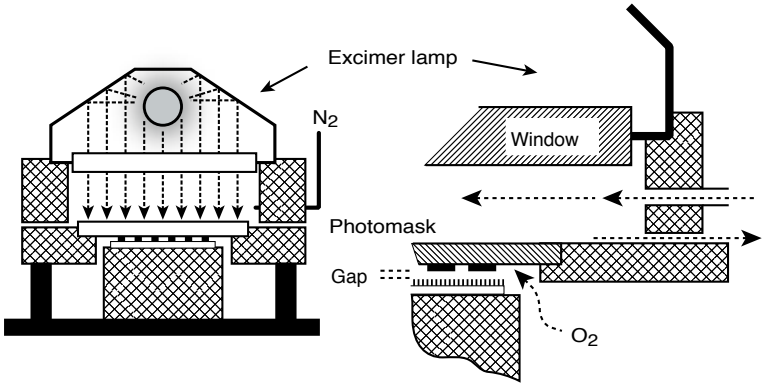

Figure 15. VUV exposure system.

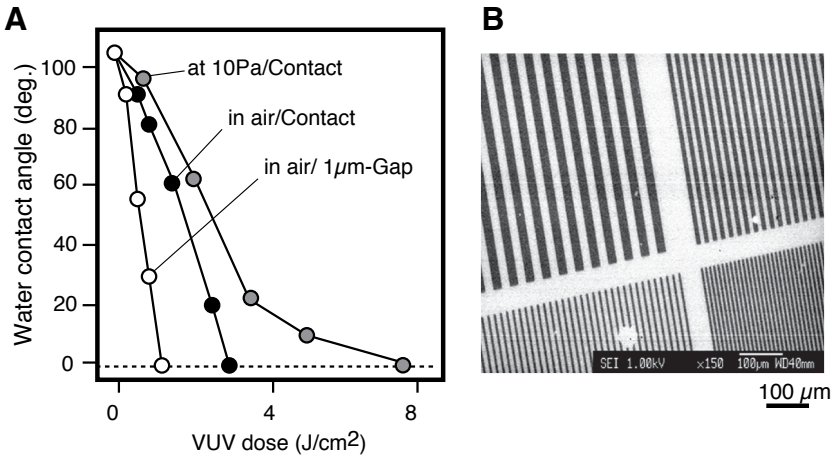

Figure 16. The performance of the VUV exposure system. A) Changes in water contact angles of ODS-SAM covered samples. B) FE-SEM image of an patterned ODS-SAM acquired at an electron energy of 1 keV.

about 8 J/cm^2 is required in order to fabricated a micropattern on ODS-SAM at a pressure of 10 Pa using the apparatus shown in Fig. 12A, as similarly to the result shown in Fig. 12D. On the contrary, a required dose for micropatterning using the VUV-system is only 3 J/cm^2 or less as indicated by the closed circles in Fig. 16A. The dose is further reduced down to near 1 J/cm^2 as indicated by the open circles, when a gap of 1 μm was located between the photomask and the sample. An example of a printed pattern on the ODS-SAM sample is shown in Fig. 16B. Fine lines of 5 ~ 20 μm wide were successfully transferred form the photomask. These patterns were observed by a field-emission scanning electron microscope (FE-SEM) based on the difference in secondary electron emission efficiencies between ODS-SAM and SiO_2 [82].

The VUV-exposure system enabled faster patterning rates. However, a several minutes are still needed in order to decompose ODS-SAM entirely. An alternative idea is necessary in order to further speed up patterning rates without increasing a power of the VUV light source. We have proposed and demonstrated the micro-photo-conversion patterning in which only top surface parts of a monolayer are photochemically modified instead of decomposing an entire monolayer [83]. As illustrated in Fig. 17A, an organosilane SAM prepared from p-chloromethylphenyltrimethoxysilane (CMPhS-SAM) was used as a sample.

The water contact angle of the CMPhS-SAM surface decreased due to VUV-irradiation from its initial value of 76° before irradiation to approximately 0° at 60 s (dose 0.56 J/cm^2). In contrast, it took 1800 s (dose = 15.1 J/cm^2) to decompose the CMPhS-SAM to the extent that its water contact angle became approximately 0°, when it was irradiated under a reduced pressure of 10 Pa using the apparatus of Fig. 12A. Figure 17B shows an XPS-C1s spectrum of CMPhS-SAM in an intermediate state before its complete decomposition, that is, irradiation for 5 s (dose = 0.046 J/cm^2). This VUV-irradiated CMPhS-SAM surface became slightly hydrophilic and showed a water contact angle of approximately 50°, probably because some amounts of polar functional groups had been formed photochemically as shown in the spectrum as a distinct shoulder at binding energies ranging from 287 to 290 eV. This should correspond to -COOH and -CHO groups.

Such an oxidized CMPhS surface covered with the polar functional groups is expected to have an affinity for the silane coupling reaction. To confirm this assumption, we exposed a VUV-patterned CMPhS-SAM sample to ODS vapor.

ODS molecules were assumed to be deposited selectively on the VUV-irradiated region and, consequently, to form a micropatterned ODS-SAM. Figures 17D and 17E show FE-SEM images of a binary CMPhS/ODS coplanar structure. Dark and bright regions correspond to the regions terminated with CMPhS and ODS, respectively. As we have reported, secondary electron emission from organosilane SAMs is strongly dependent on their molecular species. The CMPhS-SAM was darker than the ODS-SAM in FE-SEM images as a function of the electron affinity of the SAMs [82]. Therefore, the results shown in Figs. 17D-E clearly demonstrate that ODS molecules have been deposited selectively on the VUV-irradiated CMPhS-SAM surface. At present, a spatial resolution near 1 μm was achieved as demonstrated in Fig. 17E.

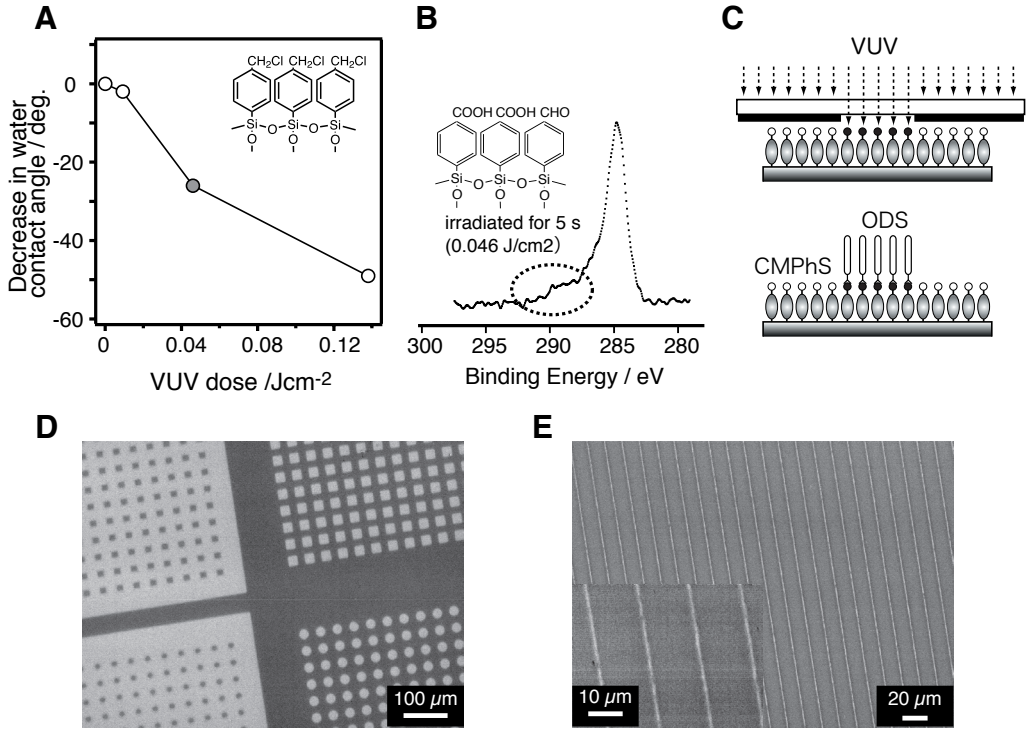

Figure 17. VUV-exposure of CMPhS-SAM. A) Decrease in water contact angle due to VUV-irradiation. B) XPS-C1s spectrum of the CMPhS-SAM irradiaed for 5 s. C) VUV-patterning of CMPhS-SAM followed by ODS treatment. D and E) FE-SEM images of the ODS/CMPhS microstructures.

5.5. Scanning probe nanopatterning of SAMs on Si

Modern microscopy technologies, which enable to obtain enlarged images of minute objects, are close relations to lithographic technologies, in which mechanisms for generation and replication of micro ~ nanometer-scale patterns are required. Scanning probe microscopy (SPM) has been a powerful means to investigate material surfaces with high spatial resolutions at nanometer scales and, in favorable cases, at atomic ~ molecular scales. Accordingly, SPM technologies have attracted much attention as nanoprocessing tools [84-91].

In order to apply SPM to nanolithography, the optimum resist material is a key factor. Among a variety of materials, organic thin films are practically important and have been frequently applied as patterning materials for lithography. Thus, the patterning of organic thin films by SPM is of special importance. However, in order to attain high spatial resolution in nanometer scale, resist films must be prepared in a thin and uniform layer. Furthermore, the films must be compatible with pattern transfer processes particularly with chemical etching. SAMs fulfill the requirements for high-resolution resist films including thickness, uniformity, patternability and compatibility to various pattern transfer processes so as to be the most promising candidate [92-98].

An ODS-SAM/Si sample surface was modified using an AFM as illustrated in Fig. 18A. In order to inject current into the sample, a DC bias voltage was applied between the conductive AFM probe and the substrate Si which served as cathode and anode, respectively. An electrically conductive probe (a heavily doped Si probe) was used. Figure 18B shows an LFM image of a patterned ODS-SAM/Si sample surface. The square feature showing a higher lateral force corresponds to the region at where current was injected from an AFM probe. From a topographic AFM image of this sample, the probe-scanned region was confirmed to protrude a few nm from the surrounding ODS-SAM/Si surface

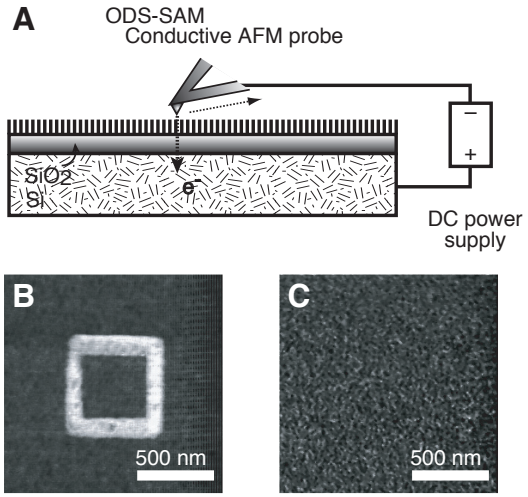

Figure 18. Current-injecting AFM lithography using ODS-SAM as a resist film. The probe was scanned at a speed of 0.1 μm/s while being pressed to the sample surface at a load force of 3 nN. A bias voltage of 10 V was applied between the probe and the substrate Si. A) Schematic illustration. B) LFM image of the ODS-SAM/Si sample current-injected in air. C) LFM image of the ODS-SAM/Si sample current-injected in vacuum at a pressure of 1.5×10^{-6} Torr.

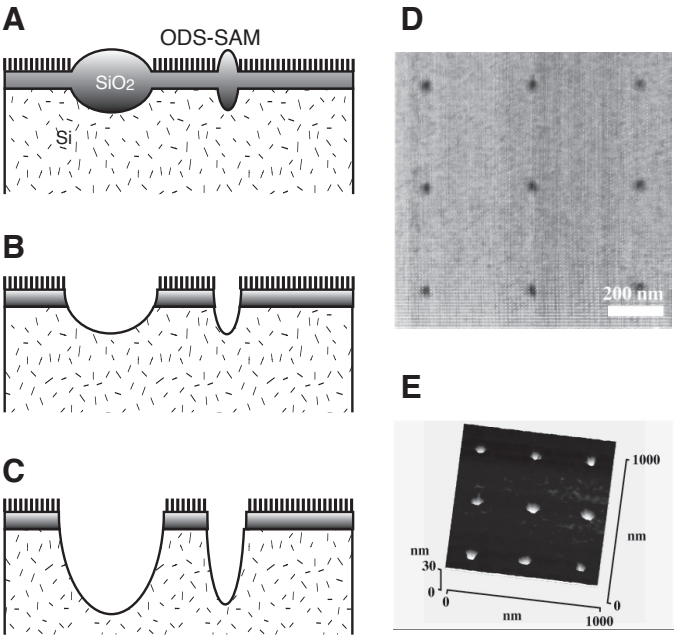

Figure 19. Pattern transfer via chemical etching. A) Patterned ODS-SAM/Si. B) oxide etching with HF (0.1%, 10 min, R.T.). C) Si etching in a solution of NH4F:H2O2:H2O = 10:3:100 (weight ratio), 1 min, R.T.). D) LFM image of a patterned sample. E) Topographic image of the etched sample.

where current was not injected. On the contrary, there are no features detectable by LFM on the ODS-SAM/Si sample scanned and current-injected in vacuum, although the same bias and load force were applied. Mechanical scratching is not a mechanism of the surface modification, since the ODS-SAM/Si is so robust that no damages were induced even at a load force of 600 nN [99]. We, thus, conclude that the ODS-SAM/Si sample was modified through electrochemical reactions proceeding in the adsorbed water column formed at the probe-sample junction as similarly to scanning probe anodization [100]. Due to these reactions, the organic molecules consisting of the ODS monolayer were anodically degraded and finally decomposed. Consequently, a lateral force contrast between the modified and unmodified regions was generated. In addition, anodization of the substrate Si occurred simultaneously so that the current-injected region protruded.

Here we demonstrate a pattern transfer process in which a pattern drawn on an ODS-SAM/Si sample is transferred into its substrate Si via chemical etching (Fig. 19). First, the sample patterned by AFM is treated in a HF solution. An LFM image of the patterned sample surface is shown in Fig. 19D. Dots of 30 nm in diameter have been formed. Due to the HF etching, oxide in the region modified by AFM is etched as illustrated in Fig. 19B. Next, the sample is further etched in a mixed solution of ammonium fluoride and hydrogen peroxide. The substrate Si is selectively etched in this solution as illustrated in Fig. 19C. Indeed, as demonstrated in Fig. 19E, nanoholes of 50 nm in diameter and 30 nm in depth are formed on the sample.

5.6. Reversible nanochemical conversion

Among the various principles behind scanning probe lithography, local oxidation as describe in Section 5.5. is the most promising way. Based on electrochemistry, local oxidation proceeds in a minute water column formed between the sample and the tip of an SPM [100]. In order to achieve reversible chemical nanopatterning based on SPM, both oxidation and reduction reactions must be manipulated.

Here we demonstrate a reversible surface modification of a SAM surface using SPM with manipulating both electrochemical oxidation and reduction reactions in a control manner [101,102]. We employed a SAM prepared from p-aminophenyl-trimethoxysilane (APhS, $H_2N(C_6H_4)Si\ (OCH_3)_3$) as a sample material. Figure 20A shows the chemical structures of the APhS molecule and the corresponding SAM. Surface-modification experiments were conducted in air using an AFM with a gold coated Si cantilever. A dc bias was applied to the Si substrate, while the cantilever grounded, in order to induce electrochemical reactions at the probe-sample junction. Kelvin-probe force microscopy (KFM) imaging was conducted using the same AFM and probe used to modify the surface.

Figures 20C and 20D show the surface-potential images of the probe-scanned APhS-SAM surfaces. The probe-scanned regions have different surface potentials compared to the as-prepared APhS-SAM surface. At a negative sample bias voltage, a bright square with a higher surface potential than the as-prepared APhS-SAM was formed, while a dark square with a lower surface potential was formed at the positive sample bias voltage. It is noteworthy that there were no

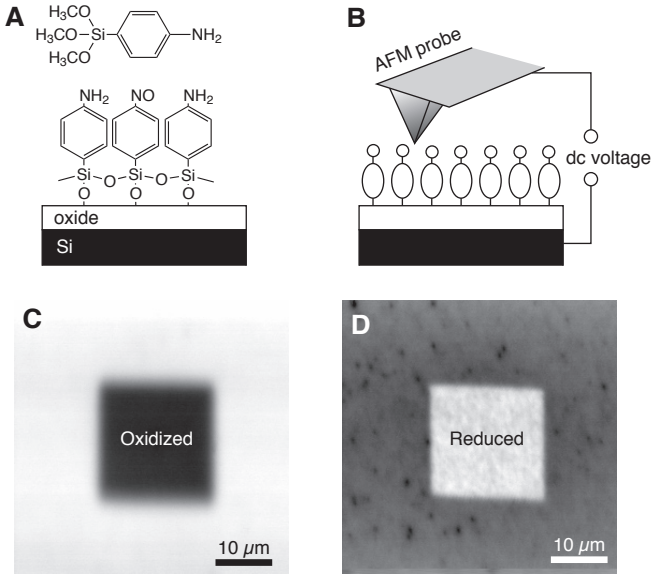

Figure 20. Sample preparation and surface modification. A) Chemical structures of APhS molecule and the corresponding SAM. A partially oxidized APhS-SAM (0.6 nm thick) was prepared on Si substrates (100 orientation, n-type, 4-6 Ωcm) covered with an 2-nm thick oxide layer. B) Schematic illustration of the surface modification procedure. KFM images of surface-modified samples at dc biases of C) +3 and D) -3 V.

apparent topographic changes in the probe-scanned regions.

The surface potentials of organic thin films are reported to be governed by their polarization states [103-106]. In an aqueous solution, the amino (NH_2) groups can be electrochemically oxidized into nitroso (NO) groups and the NO groups can be electrochemically reduced to NH_2 groups. Thus, the reduced and oxidized states of the APhS-SAM fabricated in this study are considered to have NH_2-terminated and NO-terminated surfaces, respectively. The NO-terminated SAM surface was assumed to be negatively polarized since the NO groups attract electrons from the aromatic rings that consist of the SAM. Therefore, the surface potential of the SAM shifts toward the negative direction when terminated with NO groups. This is the reason that the probe-oxidized area showed lower surface potentials than the surrounding as-prepared SAM surfaces (Fig. 20C). However, it was assumed that the NH_2-terminated surface is positively polarized, since the NH_2 groups supply electrons to the aromatic rings. The NH_2-terminated surface, that is, the reduced state of the APhS-SAM, should show a higher surface potential than the as-prepared surface (Fig. 20D). Considering the results that both reducing and oxidizing modifications could be conducted on the as-prepared APhS-SAM surface, it was most likely to be partially oxidized as schematically shown in Fig. 20A. Namely, a portion of NH_2 groups had been oxidized to NO groups during the preparation process in which APhS molecules were heated up to be

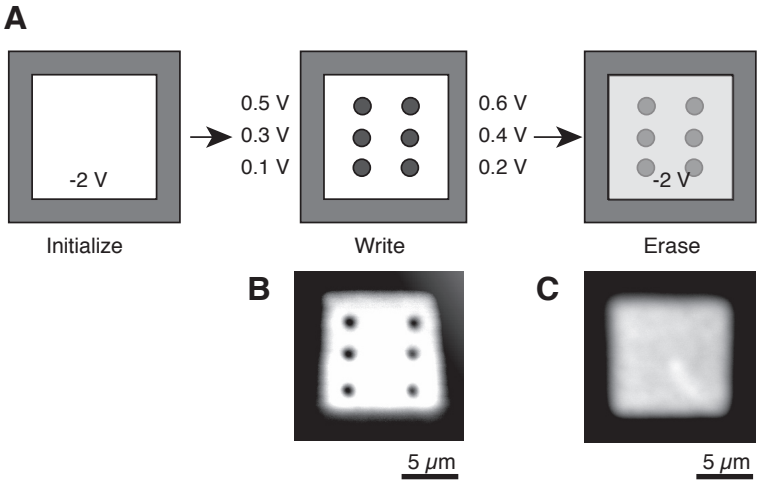

Figure 21. Reversible nanochemical conversion A) Initializing, writing and erasing. B) KFM image of an initialized 10 μm square at a dc bias of - 2 V and six dots written in the initialized square by oxidation with 1 sec pulses. Each peak voltage is indicated in figure. C) KFM image of the same area with that of Fig. 21B acquired after erasing with a reductive over-scanning at a dc bias of -2 V.

100 °C in air [101].

A writing and erasing experiment based on these oxidation and reduction mechanisms was conducted as shown in Fig. 21A. In this experiment, a 10 μm-square region on the as-prepared APhS-SAM was initially reduced at a bias of -2 V. This reduced region is appeared as the bright square feature in the KFM image as shown in Fig. 21B. Next, six oxidized dots were fabricated in this initialized area under the writing conditions as indicated in Fig. 21A. As can be seen in the surface potential image of Fig. 21B, the oxidized dots are detected as dark dots with 40 ~ 50 mV lower potentials than the initialized surface. Then, the same 10-μm square region was reduced. The KFM image of Fig. 21C indicates that the oxidized dots were successfully erased. This writing and erasing process can be repeated at least several times.

6. Some electrical properties of SAMs on Si

6.1. Surface potentials of organosilane SAMs

SAMs markedly alter surface properties of substrates, including electrical ones of substrates. For example, organosilane SAMs have been applied to control characteristics of organic field-effect transistors through the modification of the interface between an organic semiconductor layer and a gate oxide film [107]. The knowledge on dipole moments of SAMs, consequently, surface potentials of SAMs well-known to be closely related to dipole moments of the molecules consisting of the SAMs [108-110], is of primary importance for such an application.

Five types of SAMs, that is, 3,3,3-trifluoropropyltrimethoxysilane [TFPS, $CF_3(CF_2)_2Si(OCH_3)_3$] in addition to ODS, FAS, CMPhS and AHAPS as depicted in Figs. 22A-E were studied. Samples for surface potential measurements were fabricated by the procedures as shown in Figs. 22F-H. First, an ODS-SAM was prepared on Si substrates (n-type, 4 ~ 6 Ω·cm) by the vapor phase method. Next, the substrate covered with ODS-SAM was micropatterned by VUV-lithography as described in Section 5.3. In the VUV-irradiated regions, the SAM was selectively removed so that the underlying SiO_2 layer was exposed. Finally, the VUV-patterned ODS-SAM sample was treated with a different precursor. Since such a photochemically exposed oxide surface was most likely to be terminated with OH groups, it have an affinity to organosilane molecules. The second SAM (SAM-2) consisting of FAS, TFPS, CMPhS or AHAPS area-selectively formed confining to the VUV-irradiated pattern. In order to obtain surface potential differences between ODS-SAM and the other SAMs, the coplanar FAS/ODS, TFPS/ODS, CMPhS/ODS and AHAPS/ODS microstructures were observed by KFM.

Figures 23A-D show KFM images of the FAS/ODS, TFPS/ODS, CMPhS/ODS and AHAPS/ODS coplanar microstructures, respectively. Rectangular features of 5 μm × 25 μm correspond to the regions covered with a SAM other than ODS-SAM, while the surrounding area is covered with ODS-SAM. As clearly seen in Figs. 23A-C, the regions covered with FAS-SAM, TFPS-SAM and CMPhS-SAM show lower surface potentials than ODS-SAM. On the

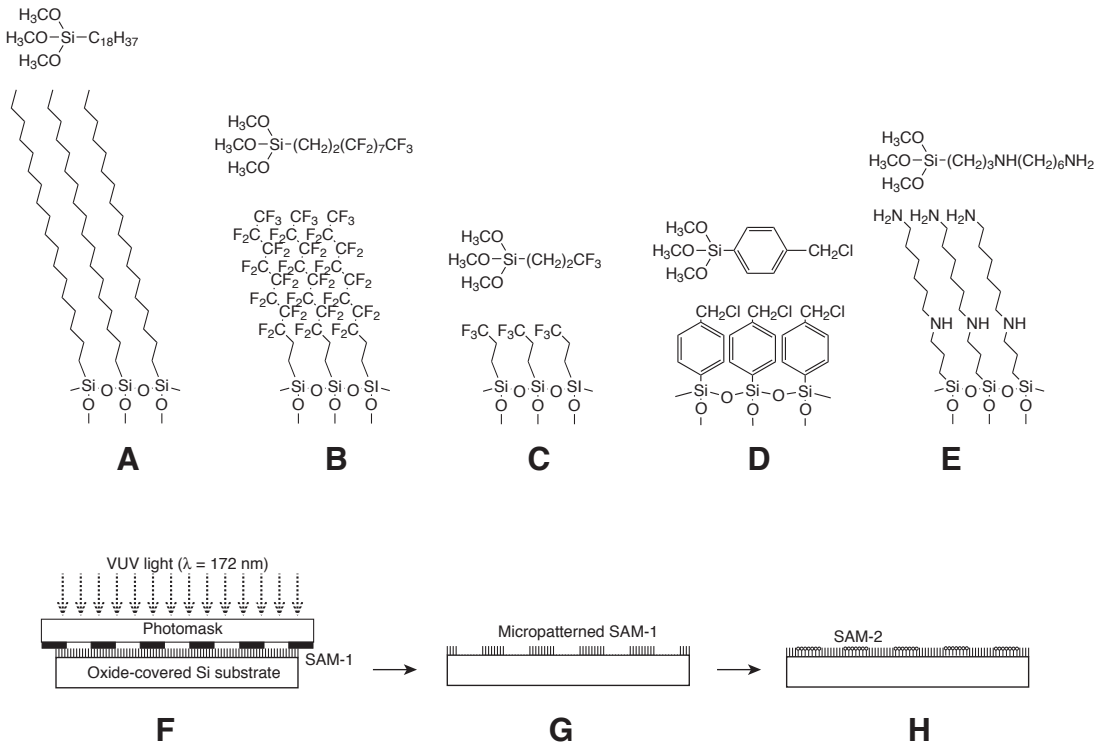

Figure 22. Chemical structures of SAMs and their precursors A) ODS-SAM, B) FAS-SAM, C) TFPS-SAM, D) CMPhS-SAM and F) AHAPS-SAM. F-H) The procedure for sample preparation.

contrary, the region covered with AHAPS-SAM, as shown in Fig. 23D, possesses a higher surface potential than ODS-SAM. The potential contrasts of the regions covered with FAS-SAM, TFPS-SAM, CMPhS-SAM and AHAPS-SAM with reference to ODS-SAM are ca. -180, -150, -30 and +50 mV, respectively. The main advantage of ODS-SAM as a reference is its hydrophobicity. Since the amount of adsorbed water, which affects measured surface potentials significantly [111,112], on ODS-SAM is small, surface potentials are reliably measured.

Here we discuss surface potential contrasts between ODS-SAM and the others. A surface potential of a SAM on a Si substrate is expressed by Eq. 2,

$$V_{SAM} = -\frac{(\phi_{subst} - \phi_{tip})}{e} + \frac{\mu}{A\varepsilon_{SAM}\varepsilon_0} + \alpha \qquad (2)$$

where ϕ_{subst} and ϕ_{tip} are work functions of the Si substrate and the KFM tip, respectively, e is the electric charge, μ is the net dipole moment directed normally to the substrate surface, A is the area occupied by each molecule, and ε_{SAM} and ε_0 are the permittivity of the SAM and free space, respectively. Eq. (1) is consist of three terms: the first is $-(\phi_{subst} - \phi_{tip})/e$ which represents the contact potential difference between the Si substrate and KFM tip, the second is $\mu/A\varepsilon_{SAM}\varepsilon_0$, which represents the dipole moment of an organic thin film derived from Helmholtz equation, the third is α which corresponds to a potential generated by trapped charges in the SiO_2 layer. The surface potential difference between the regions covered with ODS-SAM and another SAM is obtained by Eq. 3,

$$V_{SAM} - V_{ODS} = \frac{\mu_{SAM}}{A_{SAM}\varepsilon_{SAM}\varepsilon_0} - \frac{\mu_{ODS}}{A_{ODS}\varepsilon_{ODS}\varepsilon_0} \qquad (3)$$

where the first and third terms of Eq. 2 do not remain. We assumed that differences in A and ε between ODS-SAM and the other SAMs are not so significant, since the SAMs are laterally connected with an identical Si-O-Si network as shown in Fig. 3 and are formed mainly from hydrocarbons. Thus, the potential contrast is considered to be primarily governed by the difference in dipole moment.

Dipole moments of ODS, FAS, TFPS, CMPhS and AHAPS molecules were calculated using a slightly simplified model for each molecule in which each of three methoxy groups is replaced with a hydrogen atom, since the methoxy groups in the precursor molecules do not remain in the SAMs. The modeled ODS, FAS, TFPS, CMPhS and AHAPS molecule have dipole moments of 2.35, 3.41, 2.91, 2.40 and 1.04 Debye, respectively. These dipole moments incline 26.5, 25.3, 3.6, 55.1 and 12.4°, respectively, with respect to each of the molecular chains. Vertical components of the dipole moments for the model ODS and AHAPS molecules are positive, namely, the dipole moments are directing from the bottom to the top, while those for the other model molecules, i.e., FAS, TFPS and CMPhS are negative due to electron negativities of fluorine and chlorine atoms existing in their head groups. The dipole moments of the model FAS, TFPS, CMPhS and AHAPS molecules were compared with that of the ODS model with regard to their vertical components. The estimated vertical dipole moment differences ($\Delta\mu_\perp$) are as follows.

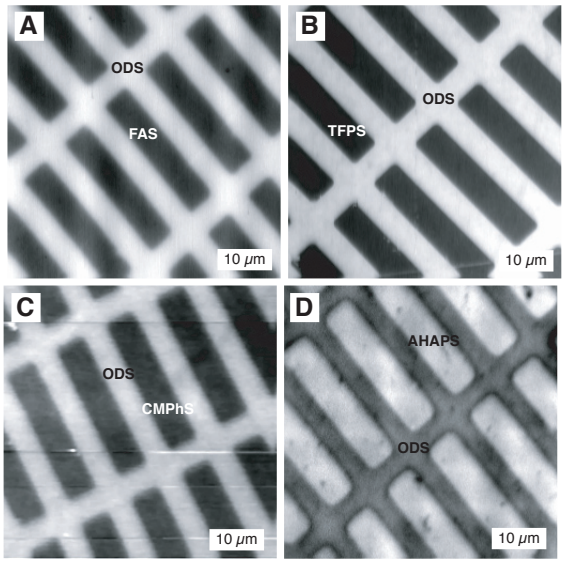

Figure 23. Surface potential images of A) FAS/ODS, B) TFPS/ODS, C) CMPhS/ODS and D) AHAPS/ODS.

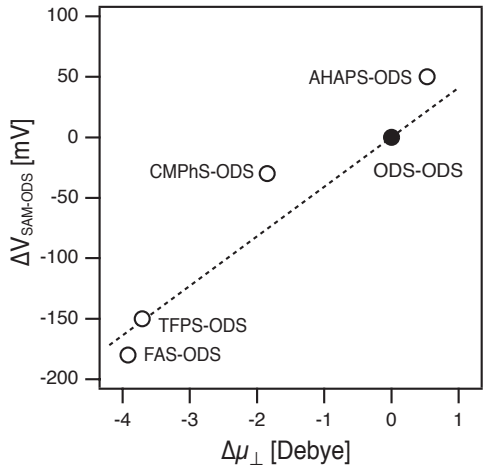

Figure 24. Relation between $\Delta\mu\perp$ and ΔV.

$$\Delta\mu\perp(\text{FAS-ODS})\ (-3.92\text{D}) < \Delta\mu\perp(\text{TFPS-ODS})\ (-3.71\text{D}) < \Delta\mu\perp(\text{CMPhS-ODS})\ (-1.85\text{D})$$
$$< \Delta\mu\perp(\text{ODS-ODS})\ (0\text{D}) < \Delta\mu\perp(\text{AHAPS-ODS})\ (+0.53\text{D}) \quad (4)$$

The order and signs of $\Delta\mu\perp$ qualitatively agree with the order and signs of the surface potential contrasts (ΔV) as shown in Fig. 24. The line indicated in Fig. 24 is the relation derived form Eq. 3 with assuming that A_{SAM} and ε_{SAM} are identical for all the SAMs. One plausible reason for the discrepancy between the experimental and calculated results is the molecular orientation in SAM, since the above discussion is based on the assumption that molecules in a SAM are aligned perpendicular to the substrate surface. It is known that SAMs are frequently constructed from inclined molecules [1]. The difference in A_{SAM} is also responsible. For example, TFPS-SAM incompletely covered a substrate compared with FAS-SAM. Since the molecular length of TFPS is much shorter than that of FAS, intermolecular interactions, which are necessary to form a densely packed monolayer, is so weak that TFPS-SAM is loosely packed.

6.2. Conductive and electroactive SAMs covalently bonded to Si

When an unsaturated hydrocarbon molecule having a carbon-carbon double bond reacts with a hydrogen-terminated Si surface, the molecule is attached to the substrate with a interfacial chemical structure of ≡Si-CH_2-CH_2- as shown in Fig. 4. Consequently, the formed SAM entirely consists of σ bondings and is essentially an electrical insulator. On the contrary, in the case of a molecule containing a carbon-carbon triple bond, a SAM with an interfacial structure of ≡Si-CH_2=CH_2- is formed. For example, phenylacetylene (PA) molecules form a π-conjugated SAM which is expected to be electrically conductive as illustrated in Fig. 25A.

This π-conjugated SAM was actually formed on a Si(111)-H surface through a chemical reaction of PA at a temperature of 180 °C [76]. Figure 25B shows a current-voltage (I-V) characteristic of a junction between the π-conjugated SAM/Si sample and a gold-coated conductive probe of AFM in addition to an I-V curve of a Si(111)-H surface as a control. The junction current on the SAM surface distinctly flows at lower substrate voltages than that on the Si-H surface. These results mean that a contact resistance between Au and π-conjugated SAM is lower than that between Au and Si-H. It has been actually demonstrated that the π-conjugated SAM is electrically conductive to some extent and electrical properties of Si surfaces can be controlled by preparing a directily-bondig SAM on the surfaces.

Redox-active molecules have an ability to store and release electric charges reversibly. SAMs of such redox-active molecules attached to silicon [112-115] are, thus, expected to be applied to solid-state memory devices. Ferrocene

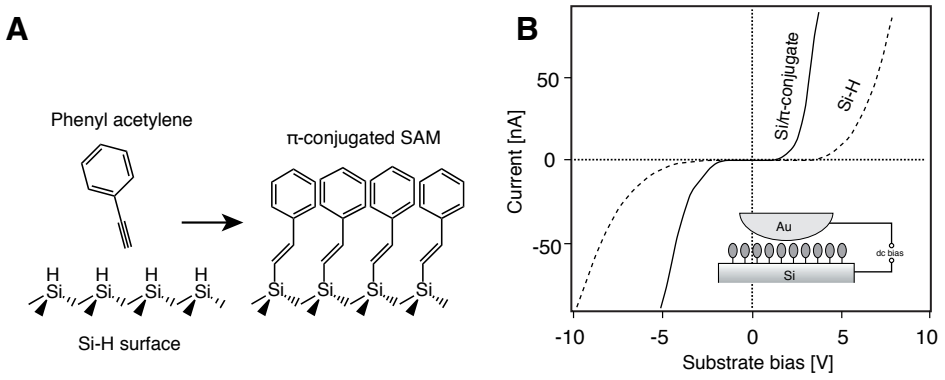

Figure 25. SAM on Si prepared from phenylacetylene. A) Chemical structures of phenylacetylene and the corresponding SAM. B) I-V characteristics of the junctions formed under an Au-coated AFM probe with the SAM-covered Si or Si-H surfaces.

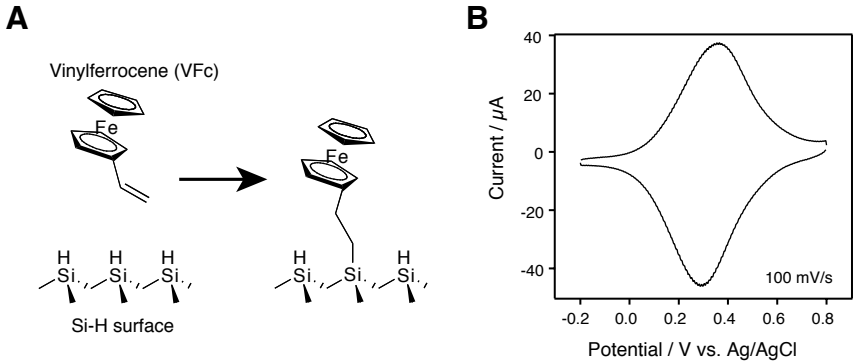

Figure 26. Immobilization of vinylferrocene molecules on Si. A) Chemical reaction scheme. B) Cyclic-voltammogram of a VFc-treated Si electrode.

has appropriate properties, such as redox activity, reversibility in redox reactions, durability in repetition of the reactions. Thus, vinylferrocene (VFc) molecules were attached to a Si(111) surface through Si-C bonds by immersing a Si(111)-H substrate to a bath of 10 mM VFc dissolved in mesitylene at 150 °C for 15 hours as schematically illustrated in Fig. 26A.

A cyclic voltammogram for the Si(111) electrode functionalized with VFc was measured in a 0.1M $HClO_4$ solution under a nitrogen purged atmosphere as shown in Fig. 26B. Oxidation and reduction peaks are observed at potentials around 0.36 V and 0.3 V, respectively. This means that ferrocenyl groups in the VFc molecules attached to Si undergo the oxidation/reduction reactions.

7. Summary and conclusion

Besides a brief introduction to general aspects of SAMs formed on various solid substrates, preparation and properties of SAMs on Si were reviewed in this chapter. Two of major methods for the fabrication of SAMs on Si were described. One is the silane coupling chemistry, that is, the chemical reactions between organosilane molecules and hydroxyl groups on a surface oxide layer of Si. Thus, an interfacial oxide layer between the SAM and Si substrate is substantially present. The other method is based on the chemical reactions of unsaturated hydrocarbon, alcohol and aldehyde with Si-H activated by thermal- or photo-excitation. By the method, the organic molecules are directly attached to bulk Si through Si-C or Si-O-C bonds. Furthermore, micro and nanopatterning of the SAMs on Si, based on VUV-light irradiation and current-injecting AFM, respectively, were described. Finally, some of electric properties of the SAMs, that is, surface potential, contact resistance and redox activity, were demonstrated.

The growth of thin films via chemisorptions of organic molecules onto solid surfaces has been a well-known phenomenon since 1940s. However, recent advances in science and technology, particularly in surface characterization and analyzing methods, have elucidated fundamental and practical aspects of SAMs, for example, their structures in molecular scales, detailed growth mechanisms and practically useful functionalities. Consequently, the research and development on SAM and its application have been markedly pushed forward. The self-assembling approach to fabricate ultra thin films using molecules as building blocks will become a crucial technology more and more as one of bottom-up nanotechnologies in surface and interface engineering with a variety of practical applications.

References

[1] A. Ulman, Chem. Rev. 96 (1996) 1533.
[2] Frank Schreiber, Prog. Surf. Sci. 65 (200) 151.
[3] S. Flink, F. C. J. M. van Veggrl and D. N. Reinhoudt, Adv. Mater. 12 (2000) 1315.
[4] J. C. Love, L. A. Estroff, J. K. Kriebel, R. G. Nuzzo and G. M. Whitesides, Chem. Rev. 105 (2005) 1103.
[5] W. C. Biegelow, D. L. Pickett and W. A. Zisman, J. Colloid Sci. 1 (1946) 513.
[6] L. O. Brockway and J. Karle, J. Colloid Sci. 2 (1947) 277.
[7] E. G. Shafrin and W. A. Zisman, J. Colloid Sci. 4 (1949) 571.
[8] E. P. Plueddemann, Silane Coupling Agents, Second Edition, (Plenum Press, NewYork and London, 1991).
[9] E. E. Polymeropoulos and J. Sagiv, J. Chem. Phys. 69 (1978) 1836.
[10] J. Sagiv, J. Am. Chem. Soc. 102 (1980) 92.
[11] M. R. Linford and C. E. D. Chidsey, J. Am. Chem. Soc. 115 (1993) 12631.
[12] J. M. Buriak, Chem. Rev. 102 (2002) 1271.
[13] A. B. Sieval, B. van den Hout, H. Zuilhof and E. J. R. Sudhoelter, Langmuir 16 (2000) 2987.
[14] S. R. Wasserman, Y.-T. Tao and G. M. Whitesides, Langmuir 5 (1989) 1074.
[15] U. Jonsson, G. Olofsson, M. Malmqvist and I. Ronnberg, Thin Solid Films 124 (1985) 117.
[16] H. Tada and H. Nagayama, Langmuir 11 (1995) 136.
[17] P. W. Hoffmann, M. Stelzle and J. F. Rabolt, Langmuir 13 (1997) 1877.
[18] H. Sugimura and N. Nakagiri, J. Photopolym. Sci. Technol. 10 (1997) 661.
[19] A. Y. Fadeev and T. J. McCarthy, Langmuir 15 (1999) 3759.
[20] A. Hozumi, K. Ushiyama, H. Sugimura and O. Takai, Langmuir 15 (1999) 7600.
[21] H. Sugimura, A. Hozumi, T. Kameyama and O. Takai, Surf. Interf. Anal. 34 (2002) 550.
[22] G. A. Husseini, J. Peacock, A. Sathyapalan, L. W. Zilch, M. C. Asplund, E. T. Sevy and M. R. Linford, Langmuir 19 (2003) 5169.
[23] T. Koga, M. Morita, H. Ishida, H. Yakabe, S. Sasaki, O. Sakata, H. Otsuka and A. Takahara, Langmuir 21 (2005) 905.
[24] G.-Y. Jung, Z. Li, W. Wu, Y. Chen, D. L. Olynick, S.-Y. Wang, W. M. Tong and R. S. Williams, Langmuir 21 (2005) 1158.
[25] A. Hozumi, H. Sugimura Y. Yokogawa, T. Kameyama and O. Takai, Colloids and Surfaces A 182 (2001) 257.
[26] M. D. Butterworth, R. Corradi, J. Johal, S. F. Lascelles, S. Maeda and S. P. Armes, J. Colloid Interface Sci. 174 (1995) 510.
[27] J. W. Goodwin, R. S. Harbron and P. A. Reynolds, Colloid Polym. Sci. 268 (1990) 766.

[28] G. A. Parks, Chem. Rev. 65 (1965) 177.
[29] M. R. Linford, P. Fenter, P. M. Eisenberger and C. E. D. Chidsey, J. Am. Chem. Soc. 117 (1995) 3145.
[30] A. B. Sieval, R. Opitz, H. P. A. Maas, M. G. Schoeman, G. Meijer, F. J. Vergeldt, H. Zuilhof and E. J. R. Sudhlter, Langmuir 16 (2000) 10359.
[31] R. Boukherroub, S. Morin, P. Sharpe, D. D. M. Wayner and P. Allongue, Langmuir 16 (2000) 7429.
[32] F. Effenberger, G. Götz, B. Bidlingmaier and M. Wezstein, Angew. Chem. Int. Ed. 37 (1998) 2462.
[33] R. Boukherroub, S. Morin, F. Bensebaa and D. D. M. Wayner, Langmuir 11 (1999) 3831.
[34] R. L. Cicero, M. R. Linford and C. E. D. Chidsey, Langmuir 16 (2000) 5688.
[35] Q.-Y. Sun, L. C. P. M. de Smet, B. van Lagen, A. Wright, H. Zuilhof and E. J. R. Sudhölter, Angew. Chem. Int. Ed. 43 (2004) 1352.
[36] W. J. Dressick and J .M. Calvert, Jpn. J. Appl. Phys. 32 (1993) 5829.
[37] A. Kumar, N. L. Abbott, E. Kim, H. A. Biebuyck and G. M. Whitesides, Acc. Chem. Res. 28 (1995) 219.
[38] Y. Xia and G. M. Whitesides, Annu. Rev. Mater. Sci. 28 153 (1998).
[39] H. Sugimura, T. Hanji, O. Takai, T. Masuda and H. Misawa, Electrochim. Acta 47 (2001) 103.
[40] S. Krämer, R. R. Fuierer and C. B. Gorman, Chem. Rev. 103 (2003) 4367.
[41] R. K. Smith, P. A. Lewis and P. S. Weiss, Prog. Surf. Sci. 75 (2004) 1.
[42] R. C. Tiberio, H. G. Craighead, M. Lercel, T. Lau, C. W. Sheen and D. L. Allara, Appl. Phys. Lett. 62 (1993) 476.
[43] J. A. M. Sondag-Huethorst, H. R. J. van Helleputte and L. G. J. Fokkink, Appl. Phys. Lett. 64 (1994) 285.
[44] N. Mino, S. Ozaki, K. Ogawa and M. Hatada, Thin Solid Films 243 (1994) 374.
[45] M. J. Lercel. H. G. Craighead, A. N. Parikh, K. Seshadri and D. L. Allara, Appl. Phys. Lett. 68 (1996) 1504.
[46] R. Hild, C. David, H. U. Muller, B. Volkel, D. R. Kayser and M. Grunze, Langmuir 14 (1998) 342.
[47] W. Geyer, V. Stadler, W. Eck, M. Zharnikov, A. Gölzhäuser and M. Grunze, Appl. Phys. Lett. 75 (1999) 2401.
[48] P. C. Rieke, B. J. Tarasevich, L. L. Wood, M. H. Engelhard, D. R. Baer, G. E. Fryxell, C. M. John, D. A. Laken and M. C. Jaehnig, Langmuir 10 (1994) 619.
[49] K. Berggren, A. Bard, J. L. Wilbur, J. D. Gillaspy, A. G. Helg, J. J. McClelland, S. L. Rolston, W. D. Phillips, M. Prentiss and G. M. Whitesides, Science 269 (1995) 1255.
[50] R. Younkin, K. K. Berggren, K. S. Johnson, M. Prentiss, D. C. Ralph and G. M. Whitesides, Appl. Phys. Lett. 71 (1997) 1261.
[51] S. B. Hill, C. A. Haich, F. B. Dunning, and G. K. Walters, J. J. McClelland, R. J. Celotta, H. G. Craighead J. Han and D. M. Tanenbaum, J. Vac. Sci. Technol. B 17 (1999) 1087.
[52] X. M. Yang, R. D. Peters, T. K. Kim and P. F. Nealey, J. Vac. Sci. Technol. B 17 (1999) 3203.
[53] T. K. Kim, X. M. Yang, R. D. Peters, B. H. Sohn, and P.l F. Nealey, J. Phys. Chem. 104 (2000) 7403.
[54] M. Zharnikov and M. Grunze, J. Vac. Sci. Technol. B 20 (2002) 1793.
[55] Y.-H. La, Y. J. Jung, H. J. Kim, T.-H. Kang, K. Ihm, K.-J. Kim, B. Kim and J. W. Park, Langmuir 19 (2003) 4390.
[56] R. Klauser, M.-L. Huang, S.-C. Wang, C.-H. Chen, T. J. Chuang, A. Terfort and M. Zharnikov, Langmuir 20 (2004) 2050.
[57] A. Kumar, H. A. Biebuyck, N. L. Abbott and G. M. Whitesides, J. Am. Chem. Soc. 114 (1992) 9188.
[58] A. Kumar, H. A. Biebuyck and G. M. Whitesides, Lanmguir 10 (1994) 1498.
[59] A. Kumar and G. M. Whitesides, Science 263 (1994) 60.
[60] Y. Xia, M. Mrksich, E. Kim, G. M. Whitesides, J. Am. Chem. Soc. 117 (1995) 9576.
[61] C. S. Dulcey, J. H. Georger, V. Krauthamer, D. A. Stenger, T. L. Fare and J. M. Calvert, Science 252 (1991) 551.
[62] D. A. Stenger, J. H. Georger, C. S. Dulcey, J. J. Hickman, A. S. Rudolph, T. B. Nielsen, S. M. McCort, and J. M. Calvert, J. Am. Chem. Soc. 114 (1992) 8435.
[63] C. S. Dulcey, J. H. Georger, M.-S. Chen, S. W. McElvany, C. E. O'Ferrall, V. I. Benezra and J. M. Calvert, Langmuir 12 (1996) 1638.
[64] S. L. Brandow, M.-S. Chen, R. Aggarwal, C. S. Dulcey, J. M. Calvert and W. J. Dressick, Langmuir 15 (1999) 5429.
[65] N. Ichinose, H. Sugimura, T. Uchida, N. Shimo and H. Masuhara, Chem. Lett. (1961) (1993).
[66] H. Sugimura and N. Nakagiri, Jpn. J. Appl. Phys. 36 (1997) L968.
[67] H. Sugimura and N. Nakagiri, Appl. Phys. A 66 (1998) S427.
[68] H. Sugimura, K. Ushiyama, A. Hozumi and O. Takai, Langmuir 16 (2000) 885.
[69] H. Sugimura, T. Shimizu and O. Takai, J. Photopolym. Sci. Technol. 13 (2000) 69.
[70] H. Sugimura, K. Hayashi, Y. Amano, O. Takai and A. Hozumi, J. Vac. Sci. Technol. A 19 (2001) 1261.
[71] H. Sugimura, N. Saito, Y. Ishida, I. Ikeda, K. Hayashi and O. Takai, J. Vac. Sci. Technol. A 22 (2004) 1428.
[72] H. Sugimura, L. Hong and K.-H. Lee, Jpn. J. Appl. Phys. 44 (2005) 5185.
[73] R. P. Roland, M. Bolle and R. W. Anderson, Chem. Mater. 13 (2001) 2493.
[74] L. Hong, H. Sugimura, O. Takai, N. Nakagiri and M. Okada, Jpn. J. Appl. Phys. 42 (2003) L394.
[75] N. Saito, Y. Kadoya, K. Hayashi, H. Sugimura and O. Takai, Jpn. J. Appl. Phys. 42 (2003) 2534.
[76] N. Saito, K. Hayashi, H. Sugimura and O. Takai, Langmuir 19 (2003) 10632.
[77] H. Sugimura, K.-H. Lee, H. Sano and R. Toyokawa, Colloids and Surfaces A, submitted

[78] N. Saito, K. Hayashi, S. Yoda, H. Sugimura and O. Takai, Surf. Sci. 532-535 (2003) 970.
[79] H. Sugimura, T. Hanji, O. Takai, K. Fukuda and H. Misawa, Materials Research Soceiy Symposium Peoceedings, 584 (2000) 163.
[80] H. Sugimura, K. Hayashi, N. Saito, L. Hong, O. Takai, A. Hozumi, N. Nakagiri and M. Okada, Trans. Mater. Res. Soc. Japan 27 (2002) 545.
[81] L. Hong, H. Sugimura, O. Takai, N. Nakagiri and M. Okada, Jpn. J. Appl. Phys 42 (2003) L394.
[82] N. Saito, Y. Wu, K. Hayashi, H. Sugimura and O. Takai, J. Phys. Chem. B 107 (2003) 664.
[83] H. Sugimura, L. Hong and K.-H. Lee, Jpn. J. Appl. Phys. 44 (2005) 5185.
[84] H. Rohrer, Jpn. J. Appl. Phys.32 (1993) 1335.
[85] P. Avoris, Acc. Chem. Res. 28 (1995) 95.
[86] H. Sugimura and N. Nakagiri, Jpn. J. Appl. Phys. 34 (1995) 3406.
[87] R. M. Nyffebegger and R. M. Penner, Chem. Rev. 97 (1997) 1195.
[88] C. F. Quate, Surf. Sci. 386 (1997) 259.
[89] H. T. Soh, K. W. Guarini and C. F. Quate, Scanning Probe Lithography, (Kluwer Academic Publishers, Boston, 2001)
[90] K. Sattler, Jpn. J. Appl. Phys. 42 (2003) 4825.
[91] D. Wouters and U. S. Schubert, Angew. Chem. Int. Ed. 43 (2004) 2480.
[92] C. R. K. Marrian, F. K. Perkins, S. L. Brandow, T. S. Koloski, E. A. Dobisz and J. M. Calvert, Appl. Phys. Lett., 64 (1994) 390.
[93] F. K. Perkins, E. A. Dobisz, S. L. Brandow, T. S. Koloski, J. M. Calvert, K. W. Rhee, J. E. Kosakowski and C. R. K. Marrian, J. Vac. Sci. Technol. B 12 (1994) 3725.
[94] H. Sugimura and N. Nakagir, Langmuir 11 (1995) 3623.
[95] H. Sugimura and N. Nakagir, J. Vac. Sci. Technol. A 14 (1996) 1223.
[96] H. Sugimura, K. Okiguchi and N. Nakagiri, Jpn. J. Appl. Phys. 35 (1996) 3749.
[97] H. Sugimura, K. Okiguchi and N. Nakagiri and M. Miyashita, J. Vac. Sci. Technol. B 14 (1996) 4140.
[98] H. Sugimura, T. Hanji, K. Hayashi and O. Takai, Ultramicroscopy, 91(2002) 221.
[99] K. Hayashi, H. Sugimura and O. Takai, Jpn. J. Appl. Phys. 40 (2001) 4344.
[100] H. Sugimura, T. Uchida, N. Kitamaura and H. Masuhara, J. Phys. Chem. 98 (1994) 4352.
[101] H. Sugimura, N. Saito, S.-H. Lee and O. Takai, J. Vac. Sci. Technol. B 22 (2004) L44.
[102] H. Sugimura, Jpn. J. Appl. Phys., 43 (2004) 4477.
[103] M. Fujihira, Ann. Rev. Mater. Sci. 28 (1999) 353.
[104] X. Chen, H. Yamada, T. Horiuchi and K. Matsushige, Jpn. J. Appl. Phys. 38 (1999) 3932.
[105] J. Lü, E. Delamarche, L. Eng, R. Bennewits, E. Myer and H-J. Güntherodt, Langmuir 15 (1999) 8184.
[106] H. Sugimura, K. Hayashi, N. Saito, N. Nakagiri and O. Takai, Appl. Surf. Sci. 188 (2002) 403.
[107] S. Kobayashi, T. Nishikawa, T. Takenobu, S. Mori, T. Shimoda, T. Mitanai, H. Shimotani, N. Yoshimoto, S. Ogawa and Y. Iwasa, Nature Materials 3 (2004) 317.
[108] H. Sugimura, K. Hayashi, N. Saito, N. Nakagiri and O. Takai, Appl. Surf. Sci. 188 (2002) 403.
[109] K. Hayashi, N. Saito, H. Sugimura, O. Takai and N. Nakagiri, Langmuir 18 (2002) 7469.
[110] O. Gershevitz, C. N. Sukenik, J. Ghabboun and D. Cahen, J. Am. Chem. Soc. 125 (2003) 4730.
[111] S. Ono, M. Takeuchi and T. Takahashi, Appl. Phys. Lett. 78 (2001) 1086.
[112] H. Sugimura, Y. Ishida, K. Hayashi, O. Takai and N. Nakagiri, Appl. Phys. Lett. 80 (2002) 1459.
[113] Peter Kruse, Erin R. Johnson, Gino A. DiLabio, and Robert A. Wolkow, Nano Lett. 2 (2002) 807.
[114] K. M. Roth, A. A. Yasseri, Z. Liu, R. B. Dabke, V. Malinovskii, K.-H. Schweikart, L. Yu, H. Tiznado, F. Zaera, J. S. Lindsey, W. G. Kuhr and D. F. Bocian, J. Am. Chem. Soc. 125 (2003) 505.
[115] Q. Li, G. Mathur, M. Homsi, S. Surthi and V. Misra, Appl. Phys. Lett. 81 (2002) 1494.
[116] R. Zanoni, F. Cattaruzza, C. Coluzza, E.A. Dalchiele, F. Decker, G. Di Santo, A. Flamini, L. Funari, A.G. Marrani, Surf. Sci. 575 (2005) 260.